

# Advances in Full Control of Electromagnetic Waves with Metasurfaces

Lei Zhang, Shengtao Mei, Kun Huang, and Cheng-Wei Qiu\*

Metasurfaces, two-dimensional versions of metamaterials, retain the great capabilities of three-dimensional counterparts in manipulating electromagnetic wave behaviors, while reducing the challenges in fabrication. By judiciously engineering parameters of individual building blocks (such as geometry, size, and material) and selecting specific design algorithms, metasurfaces are promising to replace conventional electromagnetic elements in nanoplasmonic/photonic devices. Significantly, such concept can be readily promoted to other disciplines, such as acoustics, thermal physics, and seismology. In this article, the latest advances in full control of electromagnetic waves with metasurfaces are briefly reviewed from a functionality perspective. A broad avenue towards real-life applications of metamaterials has been opened up, although they are still at their infant stage. At the end, several promising approaches are suggested to extend the applications of metasurfaces.

Regardless of the underlying mechanism of each application, all different functionalities are achieved on the basis of manipulating fundamental properties of EM phenomena during their propagation.<sup>[1]</sup> According to Fermat's principle, the transition of EM state from one to the other is an accumulation effect during wave propagation. In order to control the wavefront, conventional elements shape the phase distribution via a structural either geometry or refractive index of interfacial boundaries of two materials. However, due to the limited permittivity and permeability of natural materials, the existing EM elements are usually bulk, of multiwavelength thickness, and therefore hard to be integrated into nanophotonic

## 1. Introduction

The electromagnetic (EM) phenomenon—existing in various systems ranging from the universe to atoms, from organics to inorganics—forms one of the fundamental bases of nature. It attracts great interest, being dated back to thousands years ago. From classic picture to quantum picture, the wave-particle duality is attributed to the origin of various properties of EM phenomena, including amplitude, phase, polarization, and linear/angular momentum. Based on a continuously enriched understanding of EM phenomena, a myriad of EM-related devices become an indivisible part of our daily life. Complementarily, advances in current techniques in turn extend our understanding of EM phenomena in both breadth and depth.

and nanoplasmonic devices.

On the other hand, portable devices with highly integrated functions become one of the most preferable trends of current techniques. Their extremely suppressed volume leaves less room in integrating multiple functionalities within one design. Therefore, deep subwavelength structures being able to efficiently control EM phenomenon are continuously pursued. As a highly significant breakthrough, metamaterials provide more freedom in controlling light since they can be designed with arbitrary permittivity and permeability. Through tailoring the geometry or materials of components, many exceptional phenomena have been demonstrated, such as subwavelength imaging,<sup>[2]</sup> beam rotator,<sup>[3]</sup> invisibility cloaks,<sup>[4,5]</sup> etc. However, due to the bulk properties of 3D metamaterials, current nanofabrication techniques, such as electron-beam lithography (EBL), focused-ion beam (FIB), impose great challenges in their widespread applications especially at the visible range. Therefore, novel approaches with capability of efficiently manipulating EM wave propagation with ultrathin designs attract growing interests.

Frequency-selective surfaces (FSSs), usually consisting of periodically arranged metal gizmos with macro sizes, have been successfully applied to control EM wave at radio frequencies half century ago.<sup>[6]</sup> Whereas, in the past few years, we witness the rapid development in 2D metamaterial, dubbed as metasurface, due to its subwavelength dimension along wave propagation direction, which extremely simplifies the requirements in sample fabrication, meanwhile, retains powerful functionalities in controlling the propagating properties of EM waves at visible and infrared (IR) frequencies. By introducing an abrupt phase discontinuities at surface of metal/dielectric

Dr. L. Zhang, Mr. S. Mei, Prof. C.-W. Qiu  
Department of Electrical and Computer Engineering  
National University of Singapore  
Singapore 117583, Singapore  
E-mail: eleqc@nus.edu.sg

Mr. S. Mei, Prof. C.-W. Qiu  
Graduate School for Integrative Sciences and Engineering  
National University of Singapore  
Centre for Life Sciences (CeLS)  
#05-01, 28 Medical Drive, Singapore 117456, Singapore

Dr. K. Huang  
Institute of Materials Research and Engineering  
Agency for Science  
Technology and Research  
3 Research Link, Singapore 117602, Singapore



DOI: 10.1002/adom.201500690

structures, metasurfaces are able to realize extraordinary light manipulations, such as light bending,<sup>[7–11]</sup> focusing,<sup>[12,13]</sup> wave plate,<sup>[14–16]</sup> vortex beam generation<sup>[7,9,16,17]</sup> and hologram.<sup>[18–20]</sup> Significant achievements lead to more flexibility in designing nanophotonic and nanoplasmonic devices. Furthermore, with the ultrathin design and isolated control unit, it is promising to integrate multiple functionalities into one system.

From a more general perspective, plasmonic/photonic nanostructures could also be termed as metasurfaces due to their extraordinary capabilities in engineering various linear/non-linear light-matter interactions, which go beyond natural materials.<sup>[21–23]</sup> However, they are mainly employed to engineering near field with a uniform array assembled by identical unit cells. In contrast, applications of the emerging metasurfaces concentrate to manipulate EM wave propagations with spatially varying unit cells. One may find a more general discussion on metasurfaces including both identical and varying building blocks in other reviews.<sup>[24–26]</sup>

Here, we focus on the recent achievements in metasurfaces with a narrower definition, being able to fully manipulate the propagation behavior of EM waves, including amplitude, phase, polarization, and linear/angular momentum. The underlying mechanisms for metasurface design will be discussed by introducing several illustrative structures in the second part. Then, applications of metasurfaces with various functionalities will be discussed in the third part. At last, a brief conclusion and outlook of the ultrathin metamaterials is given.

## 2. Types of Phase Discontinuities Generated within Subwavelength Space

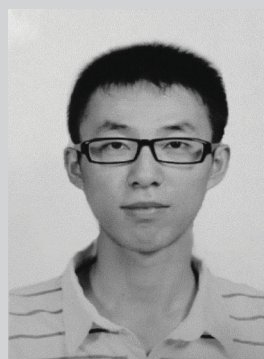
In comparison with accumulation-type phase and amplitude modulation, wave-matter interaction affords a substantial approach to control both quantities in an abrupt manner, which can be engineered with a variety of parameters, such as shape, geometric dimension, configuration and material of the constitute structures, as well as the complex surrounding environment. For example, localized surface plasmon resonances (LSPRs) have been extensively investigated as an efficient light-matter interaction process, which is formed by a dipole-like collective oscillation of electrons at the surface of metallic nanoparticles. Its resonant wavelength can be well predicted with  $\lambda_{\text{eff}} = 2L/n_{\text{eff}}$ , where  $L$  is the lateral length along electric field direction and  $n_{\text{eff}}$  is the effective refractive index of environment.<sup>[27,28]</sup> Determined by the length and material, the impedance of this oscillator is able to transit from capacitive, to resistive, and to inductance across a resonance, which leads to a  $0$ -to- $\pi$  phase shift.<sup>[29]</sup> However, full control of EM wave requires a  $2\pi$  phase variation. Fortunately, many fascinating candidates can meet the requirements. The relationship between individual building blocks and its corresponding phase or amplitude response can be well-defined via numerical simulations or theoretical predictions. Several representative examples are shown in **Figure 1**.

Besides the ultrathin thickness, another remarkable feature of metasurfaces is that all the controllabilities are mainly determined by isolated subwavelength structures. Through arranging those structures following specific target amplitude and phase distributions, one novel avenue towards to ultra-compact



**Lei Zhang** is currently a research fellow at the Department of Electrical and Computer Engineering, National University of Singapore. He received his bachelor's degree in physics from Northwest University, his master's degree in optics from Xi'an Institute of Precision Mechanics and Optics of Chinese Academy

of Science, and his PhD degree in Physics from the Chinese University of Hong Kong. His research interests are focused on metasurfaces, plasmonic and photonic resonance, and plasmon-based light-matter interactions as well as their applications to light emission, color display, sensing, etc.



**Shengtao Mei** is currently a PhD student at Graduate School for Integrative Sciences and Engineering (NGS) & Department of Electrical and Computer Engineering, National University of Singapore. He received his bachelor's degree in optics from Zhejiang University. His research interests are

focused on metasurfaces, orbital angular momentum of light (OAM), optical diffraction theory, and light-matter interactions.



**Kun Huang** is a research scientist at Institute of Materials Research and Engineering, A\*STAR, Singapore. He got his bachelor's degree in optics from Wuhan University and PhD degree in optics from University of Science and Technology of China. His research interests are

optics, nanophotonics, and their applications in optical nanofocusing, super-resolution imaging, metasurface holography, nanostructured vortex generators, and beam steering.

devices relying on wave control have been opened up. In the following, some representative examples of recent advances in full control of EM wave with metasurfaces are introduced.

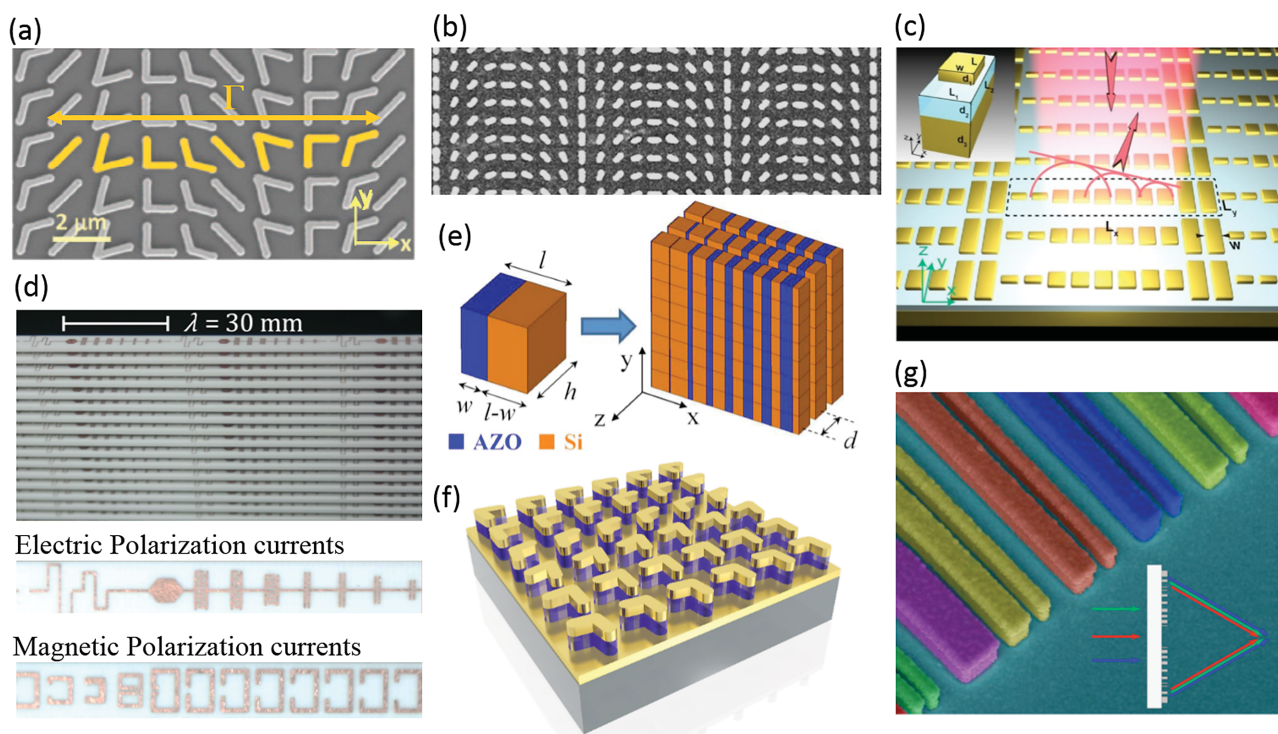


**Figure 1.** Different types of building blocks for metasurface design. a) V-shaped nanoantennas used to control the propagation of linearly polarized EM waves, which have been utilized to demonstrate wave bending, lens, QWP, vertex beam generation, etc. Reproduced with permission.<sup>[7]</sup> Copyright 2011, American Association for the Advancement of Science (AAAS). b) PB phase based metasurface realized with rotated nanorods. Reproduced with permission.<sup>[9]</sup> Copyright 2012, American Chemical Society (ACS). c) MIM metasurfaces consisting of nanorods atop with varying lengths can manipulate reflected wave with high efficiency. Reproduced with permission.<sup>[10]</sup> Copyright 2012, ACS. d) Wave manipulation with Huygens' metasurface. Reproduced with permission.<sup>[56]</sup> Copyright 2013, American Physical Society (APS). e) Full wave control realized with MTA. Reproduced with permission.<sup>[48]</sup> Copyright 2013, APS. f) Schematic of bilayer plasmonic metasurface. g) Achromatic metasurface with each unit cell consisting of two Si nanowires. Reproduced with permission.<sup>[66]</sup> Copyright 2015, ACS.

## 2.1. Phase Discontinuity Arising from Hybrid Mode

In the pioneering works of metasurfaces, V-shaped nanoantennas were first proposed and experimentally demonstrated to control the propagation of linearly polarized light at mid-infrared (MIR) range.<sup>[7,14]</sup> Soon after, it was extended to the near-infrared (NIR) range.<sup>[8]</sup> Interestingly, it should be emphasized that only the cross-polarized light is engineered with an anomalous behavior while the co-polarized counterpart propagates normally. The peculiar control over light propagation arises from field cross-projection via two closely packed arms. A V-shaped antenna supports a symmetric mode when the electric field is polarized along its diagonal axis and an anti-symmetric mode when the electric field is polarized along the orthogonal direction. Under the proper polarized illumination, the weight of two modes in the total resonance could be modified at will. The amplitude and phase of the out-coupling radiation with cross-polarization can thus be readily tailored through tuning the arm length and angle between two arms, as well as orientation of V-shaped antennas (Figure 1a). Importantly, due to the involvement of two strongly coupled arms, the V-shaped antennas could offer larger scattering amplitudes in comparison with simple rectangular rod.<sup>[30,31]</sup> By spatially positioning these particles, various functionalities have been achieved.<sup>[7,8,12,14,18]</sup> Similar functionalities were accomplished

via Babinet-inverted V-shaped nanoapertures perforated in gold films, which have even better signal-to-noise ratio (SNR) by blocking the copolarized component.<sup>[32,33]</sup>

## 2.2. Pancharatnam–Berry Phase

Later, gold nanorods were proposed to manipulate the phase profile of circularly polarized (CP) light by employing Pancharatnam–Berry (PB) phase (Figure 1b).<sup>[9,34,35]</sup> As the pioneer, Hasman et al. have demonstrated conversion of polarization state and beam splitting with space-variant metal or dielectric gratings at wavelength 10.6 μm.<sup>[36,37]</sup> Fainman et al. have also realized computer-generated holograms (CGHs) with similar structures at NIR range.<sup>[38]</sup> The beauty of this approach lies in the linear dependence of phase delay  $\phi$  on the orientation angle  $\theta$  of each nanorod, i.e.,  $\phi = \pm 2\theta$ , with the sign determined by the polarity of incident light. Moreover, the scattering amplitude remains the same due to the unchanged geometry size of each unit. Thereafter, more sophisticated designs were proposed to improve the manipulation efficiency and enable more exceptional manipulations.<sup>[39,40]</sup> Because of the geometrical nature of the PB phase, such concept can be easily extended to other frequency.<sup>[41–43]</sup> It is noted that the PB phase can only be imparted to CP light. Significantly, when a linearly polarized

light is incident, two types of CP lights will have opposite phase delay. By utilizing the polarization-dependent phase response, devices based on the PB phase have the capability of controlling two waves with opposite polarities in different manners, such as dual-polarity meta-lenses<sup>[44,45]</sup> and polarization switchable holograms.<sup>[46,47]</sup>

However, the manipulation efficiency of such single non-magnetic metasurfaces made of passive materials, either V-shaped nanostructures or PB phase metasurfaces, suffers from a theoretical upper limit 25%, which thus restricts their practical applications.<sup>[48]</sup>

### 2.3. Phase Discontinuity Arising from Gap Mode

In order to boost up the manipulation efficiency, complex mechanisms such as mode coupling and magnetic resonance, have to be involved. As shown in Figure 1c, high efficiency reflected wave control was demonstrated with metal–insulator–metal (MIM) nanostructures. From the point view of mode coupling, this MIM design can be understood as strong coupling between dipole-like LSPR atop and its image.<sup>[1,49]</sup> A magnetic resonance will be created with strong magnetic field confined inside the dielectric layer, which is usually termed as a gap mode. Phase delay can be flexibly controlled through varying the dimension or orientation of nanoparticles atop.<sup>[10,13,20,50]</sup> By blocking transmission with an optically thick metal substrate, such design is able to manipulate reflected light with an efficiency as high as 80% over a broad bandwidth. If anisotropic nanoparticles are employed as building units, polarization-dependent phase delay can also be encoded within one design.<sup>[51]</sup> Instead of geometric size variation, recently, it was shown that by rotating the orientation of nanorods atop, the PB type phase control can also be attained with an efficiency larger than 80% by combining with MIM design.<sup>[20]</sup>

Besides the high efficiency reflection control, by reducing the thickness of metallic substrate less than its skin depth and adhering two same structures back-to-back together, a high transmission has been achieved within a broadband frequency.<sup>[52]</sup> It was also used to demonstrate anomalous light propagation covering almost the entire visible band with efficiency beyond the theoretical limit of single non-magnetic metasurfaces.<sup>[53]</sup>

### 2.4. Huygens' Metasurface

Based on Huygens' Principle, the new wavefront is determined by the sum of secondary wavelets generated by the all the points on a previous wavefront. Recently, inspired by the Huygens' principle, another type of metasurface was proposed by employing both fictitious electric and magnetic polarization currents as the secondary sources.<sup>[54,55]</sup> To realize such control, polarizable particles with surface electric and magnetic polarizabilities  $a_{e,m}^{eff}$  will be spatially arranged across a 2D surface. The relation between surface polarizability and equivalent electric and magnetic surface currents can be expressed as:<sup>[56]</sup>

$$\vec{J}_s = j\omega a_e^{eff} \vec{E}_{t,vs} \Big|_s, \vec{M}_s = j\omega a_m^{eff} \cdot \vec{H}_{t,vs} \Big|_s, \quad (1)$$

where  $\vec{E}_{t,vs}|_s$  and  $\vec{H}_{t,vs}|_s$  represent the average electric and magnetic fields tangential to the surface  $S$ . As shown in Figure 1d, by stacking multiple boards consisting of two types of polarization currents, reflectionless sheets were experimentally demonstrated at microwave and NIR ranges.<sup>[56,57]</sup> Moreover, by distributing bianisotropic polarizable particles in a nonperiodic manner, polarization control could be performed with beam shaping.<sup>[58]</sup>

### 2.5. Metatransmit-Array

In a parallel effort, based on nano-circuit model, a metatransmit-array (MTA) was proposed to full control of the transmitted wave by stacking three closely spaced inhomogeneous metasurfaces (Figure 1e).<sup>[48]</sup> Each layer was composed of a plasmonic portion and a dielectric portion, connected in shut alternatively. The phase control and amplitude can be engineered independently through adjusting the filling ratio and the associated reactance once the impedance matches with the host environment. An ideal efficiency can be expected if low-loss materials are employed. By locally tailoring the parameters, MTA is potentially promising to be applied to achieve other EM wave functionalities.

### 2.6. Bilayer Metasurfaces

For single-layer metasurfaces with infinitesimally thin thickness, only transverse electric (magnetic) currents could be induced on nanoparticles (nanoapertures). The radiation symmetry results in a theoretical upper limit to the anomalous transmission. Therefore, a single ultrathin metasurface is incapable of improving manipulation efficiency of transmitted light.<sup>[48]</sup> However, such limit tends to be transcended by breaking the radiation symmetry with a finite-thickness (yet subwavelength) metasurface, for instance, a bilayer design consisting of V-shaped particles and their Babinet-inverted apertures (Figure 1f), where a transverse electric current and a transverse magnetic current are supported on the top and bottom layers consisting of structures with subwavelength lateral sizes, respectively.<sup>[59]</sup> The bilayer metasurface thus results in discontinuities on both transverse magnetic field and transverse electric field, respectively. By breaking the radiation symmetry with structural asymmetry, a full control of transmitted light with higher efficiency becomes possible.

In previous designs as listed above, couplings among adjacent unit cells are usually negligible and each unit cell could be designed individually. On the contrary, in the bilayer metasurfaces, strong intra-layer couplings among adjacent unit cells should be taken into account due to their extremely small lateral distance. Furthermore, different from previous multilayer designs, such as Huygens' metasurfaces and metatransmit-array, the separation between two layers is at deep subwavelength scale (one tenth of the operation wavelength), which also gives rise to strong inter-layer couplings. Because of the strong intra- and interlayer couplings, all the subunit cells of the bilayer metasurface are needed to be optimized as a whole. Herein, higher manipulation efficiency of anomalous

transmission, relative to single layer metasurfaces, must be attributed to the coupling effects.

## 2.7. Achromatic Metasurfaces

Chromatic dispersion is another vital issue but inevitable challenge of existing designs, which also happens to both refractive optics and diffractive optics. Even though broad operation bandwidth has been achieved with metasurfaces, chromatic aberration still occurs due to the intrinsic dispersive behavior of resonance-induced phase change. To eliminate such aberration, a wavelength-independent phase delay is required to compensate the counterpart during wave propagation. Previously, in order to obtain a broad band response, multiple modes resonant at difference wavelengths are combined either transversely or longitudinally to form a super unit cell.<sup>[60–64]</sup> Similarly, by composing two coupled rectangular dielectric resonator within one unit cell (Figure 1g), silicon metasurface has been demonstrated to enable deflecting or focusing multiply wavelengths achromatically.<sup>[65,66]</sup> It further broadens the capabilities of metasurfaces and suggests an unparalleled approach to circumvent the stubborn limitation of existing optical elements.

## 2.8. Material Concerns

Even though great achievements in wave control have been realized with the aforementioned metasurfaces, inclusion of metallic component inevitably introduces significant ohmic loss especially at visible and NIR frequencies. Alternatively, the well-established Mie theory predicts that high-refractive-index materials, such as silicon (Si), titanium dioxide (TiO<sub>2</sub>) and germanium (Ge), could provide one appealing solution to the issue of loss by supporting both electric and magnetic resonances,<sup>[67]</sup> which were not realized until recently in NIR and visible light.<sup>[68,69]</sup> Such capabilities were also extended to full control of both reflection and transmission.<sup>[16,70]</sup> By replacing high-loss metal parts with silicon counterparts, broadband linear polarization conversion and optical vortex generation have been demonstrated experimentally.<sup>[17,71,72]</sup>

The emerging 2D materials could also be excellent candidates to be patterned as metasurfaces. For instance, graphene has been employed to generate plasmonic resonance with lower loss than metal counterpart.<sup>[73–76]</sup> By tailoring the geometric size of each unit, along with the controllable dielectric properties, 2D material metasurfaces are capable of realizing active resonance behaviors within a broad bandwidth.

## 3. Properties of EM Wave Control with Metasurfaces

### 3.1. Beam Deflector and Meta-Lens

Conventional beam control elements, such as prisms and lenses, based on the phase accumulation along the optical path, suffer from bulky size, larger than operation wavelengths. In contrast, by introducing localized resonances, arbitrary phase

delay can be gained by tailoring the lateral dimension of structures while the thickness is at the sub- or even deep-sub-wavelength scale. As such, the material properties drop to the second place. **Figure 2** shows several typical examples of beam deflectors and meta-lenses.

In order to deflect an incident plane wave into a desired direction, a linear phase variation is necessary to modify the incoming wavefront. V-shaped nanostructures and nanobars were first proposed to realize the transmitted wavefront control of linearly and CP light, respectively.<sup>[7–9]</sup> However, their manipulation efficiencies were hard to meet practical applications. By using the bilayer structure, the manipulation efficiency of anomalous transmitted light with cross polarization was improved to 17% (36%) in experiment (simulation) covering the long end of visible light, which resulted from the strong intra- and interlayer coupling among adjacent unit cells.<sup>[59]</sup> To further improve the manipulation efficiency, based on MTA structures, reflected light was completely suppressed (Figure 2a), by judiciously selecting the filling ratio and reactance of building blocks, in the meantime, ensuring impedance matching to the environment. The achieved anomalous transmission efficiency was as high as 70% at a wavelength of 3 μm in simulations when the ohmic loss was minimized.<sup>[48]</sup> Comparable light bending were also demonstrated with Huygens's metasurface experimentally, with which the manipulation efficiencies were as high as 90% and 30% at microwave and NIR range, respectively.<sup>[56,57]</sup> However, the inherent high ohmic loss of metals still confines metal-based designs, especially at the visible range. In contrast, high-index dielectrics become appealing due to their low loss. More significantly, coexisting of electric and magnetic resonances within one structure facilitates almost completely suppressing the resonant reflection via their destructive interference and then results in an improved transmission. Lately, such efficiency was increased to 45% at a wavelength of 715 nm for copolarized wave control,<sup>[11]</sup> while to 72% at a wavelength of 915 nm for cross-polarized wave control.<sup>[17]</sup> On the contrary, the efficiency limit in the anomalous reflection was well overcome, for instance, 80% with a bandwidth 750–900 nm by using MIM structures, where transmission was blocked by the metal substrate with thickness much larger than skin depth.<sup>[10]</sup>

Usually, reflection and refraction occurs in the incident plane, defined by the incident and normal direction of interfacial boundaries. However, out-of-plane reflection and refraction is also desirable for 3D beaming applications. Besides using bulk anisotropic materials, it was proposed that either an inhomogeneous source or 3D photonic crystals with anisotropic band structures can realize out-of-plane refraction.<sup>[77,78]</sup> In fact, according to the generalized Snell's law, by imparting a tangential wave vector to the incident light, anomalous reflection and refraction can be realized in a non-coplanar plane, where the incidence plane was at an arbitrary angle respect to the phase gradient (Figure 2b).<sup>[79]</sup>

Since the phase control is only dependent on the isolated subwavelength antennas, metasurfaces are also flexible to be spatially arranged for even advanced functionalities, for example, flat lenses shown in Figures 2c–e.<sup>[12,44,45]</sup> To converge a planar wavefront into a spherical one at a distance  $f$  from the lens, a phase profile  $\varphi_L(x, y) = 2\pi/\lambda \left( \sqrt{X^2 + Y^2 + f^2} - f \right)$  should

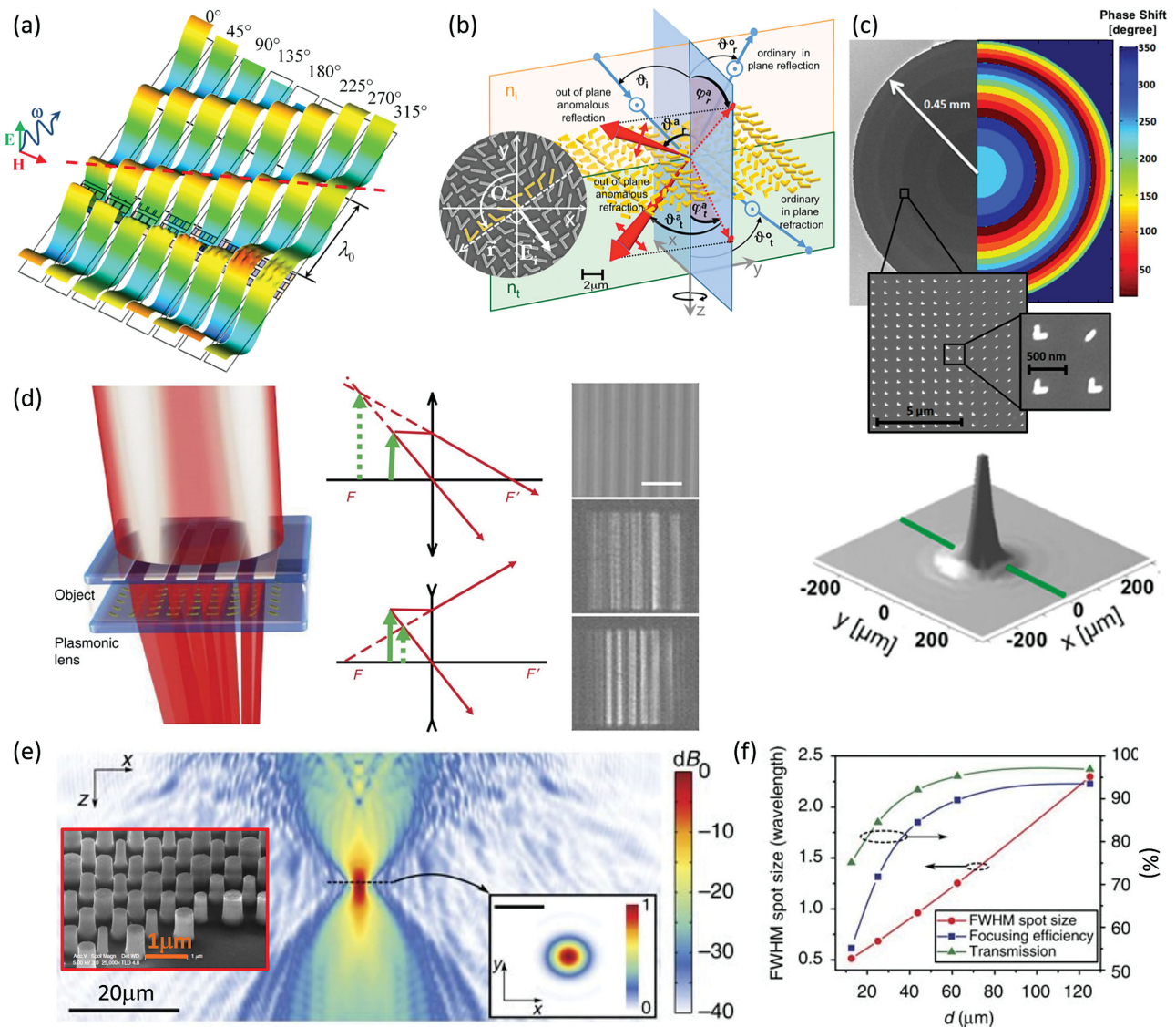


**Figure 2.** Beam deflector and meta-lens realized with metasurfaces. a) In-plane wave bending realized with three-layer design by MTA. Reproduced with permission.<sup>[48]</sup> Copyright 2013, APS. b) Out-of-plane wave bending realized with V-shaped nanoantennas. Reproduced with permission.<sup>[79]</sup> Copyright 2013, ACS. c) Flat focusing lens with consisting of V-shaped nanoantenna array. Reproduced with permission.<sup>[12]</sup> Copyright 2012, ACS. d) Dual-polarity metalens for visible light realized with PB phase metasurface. Reproduced with permission.<sup>[44]</sup> Copyright 2013, Nature Publishing Group (NPG). e, f) A meta-lens with high NA and large efficiency based on Si transmit-arrays (inset: side-view of the sample) and f) the tailorable focusing performance. e, f) Reproduced with permission.<sup>[71]</sup> Copyright 2015, NPG.

be imparted to the incident wavefront. The focusing ability depends on the numerical aperture  $NA = \sin[\tan^{-1}(D/2f)]$ , where  $D$  is the diameter of the lens. Therefore, it is straightforward to achieve good focusing performance by covering more  $2\pi$  periods.<sup>[13]</sup>

It also shows that the metasurface-based flat lens could be designed to be immune from monochromatic aberrations which need to be circumvented with quite complex optimization techniques during the fabrication of conventional refractive optical elements. It facilitates design of a high NA flat lens without aberrations even under nonparaxial conditions. In the fields of microscopy and other imaging systems such ultrathin flat lens can find relevant applications. Moreover, metasurfaces are also used to design axicons, a specialized type of

lenses, being able to perform as a hollow beam generator or a Gaussian-to-Bessel beam transformer, which can be applied in eye surgery, optical trapping, microscopes, and telescopes. For an axicon with angle  $\beta$ , a conical phase delay is required to imposed to the incident wave, which can be expressed as  $\varphi_A(x, y) = 2\pi/\lambda(\sqrt{X^2 + y^2} \sin \beta)$ <sup>[12]</sup> Figure 2c presents an axicon realization with V-shaped antennas based on cross-polarization effect at MIR frequencies.<sup>[12]</sup> Similar functionality has also been realized with Huygens' surface, where an incident Gaussian beam was transformed into a Bessel beam while maintaining the polarization with a transmittance beyond 99%.<sup>[44]</sup>

In addition to the functionality of conventional lenses, a counter-intuitive dual-polarity flat lens by using PB phase units can produce handedness-controllable magnified and

de-magnified images (Figure 2d).<sup>[44]</sup> That is to say, both the focusing and defocusing functionalities can be integrated into the same flat lens which responds to right CP light and left CP light, respectively. One drawback of these flat lenses is that the focusing light always mixed with the incident background light, which needs to be filtered out by additional polarizer/wave plate. Later, Babinet-inverted nanoapertures were developed to overcome such drawback, where a high SNR was achieved by blocking the copolarized light with opaque metal film.<sup>[32,33]</sup>

The manipulation efficiency of plasmon-based metasurfaces, either beam deflectors or meta-lenses, is far from being applied practically.<sup>[80,81]</sup> However, such issue is gradually being solved with semiconductors or high-index dielectrics.<sup>[11,16,17,72,82]</sup> A subwavelength-thick lens with high NA was reported based on high-contrast transmitarrays (Figure 2e).<sup>[71]</sup> The measured performance was summarized in Figure 2f, where the focusing efficiency was up to 42% with a spot size  $0.57 \lambda_0$  at an operation wavelength  $\lambda_0$  of 1550 nm. In addition, the design is polarization-insensitive due to isotropically local scattering effect of each silicon post. It is believed that this manipulation mechanism can be easily executed with polarization-sensitive responses by using anisotropic structures such as ellipses and rectangles.

### 3.2. Polarization Control

Polarization is another essential characteristic of EM waves with a wealth of applications in display, industry test and life science microscopy. In particular, besides the reduction of geometric dimension of each pixel, polarization states provide an alternative approach to multiply the optical information storage. Control of polarization states has thus long been pursued by different disciplines. Conventional polarization controllers, such as quarter wave plate (QWP), half wave plate (HWP) and polarization rotator (PR), are hard to meet the requirements in lab-on-chip systems due to the involvement of bulk materials, such as birefringence crystals. Its dispersive nature also makes it inherently narrow band operation. Benefiting from the extremely reduced thickness and flexible phase control, metasurfaces become appealing to supersede the conventional polarization controllers to be applied to miniaturized devices.

Over the past few years, diverse designs have been proposed to achieve efficient polarization alteration ranging from visible light to microwave.<sup>[14,15,83–89]</sup> Anisotropic structures, such as T-, C- and L-shaped structures and split rings, are widely used to tailor the phase difference of two orthogonal electric field components.<sup>[15,40,90–92]</sup> For instance, a QWP based on a metasurface consisting of phased antenna arrays is shown in Figure 3a. The unit cell contains two sub-units, which support two co-propagating waves with equal amplitude but orthogonal linear polarizations. An offset-dependent phase difference facilitates to generate controllable polarization states. The required  $\pi/2$  phase difference is added to two co-propagating waves by offsetting a  $\Gamma/4$  between two sub-units, where  $\Gamma$  is the length of the subunit. In addition, due to a phase gradient introduced along period direction, the produced CP light propagates at a deflection angle  $\theta_t = \arcsin(\lambda/\Gamma)$  which generates a background-free QWP. A high degree of circular polarization ( $>0.97$ ) is generated

within a broad bandwidth 5–12  $\mu\text{m}$ .<sup>[14]</sup> However, it should be noted that such wavelength-dependent deflection angle of CP light may have limitations to its practical applicability. Furthermore, since the phase difference is only imparted to the cross polarized electric field component with this ultrathin design, the overall conversion efficiency is capped at a maximum of 25%.<sup>[48]</sup> To overcome the efficiency limit, a T-shaped nanostructure consisting of two closely spaced nanorods was proposed (Figure 3b).<sup>[15]</sup> Distinctly, the achieved efficiency of QWP was as high as 50% covering a broad bandwidth 615–835 nm, where the additional phase delay results from the detuned resonances of two nanorods by tailoring their lengths. The measured degree of linear polarization (DoLP) and angle of linear polarization (AoLP) are remarkably large under CP illumination (Figure 3c). Recently, through introducing coupling between two layers with orthogonal punched apertures, acting as two linear polarizers, a HWP was demonstrated in both NIR frequency (conversion efficiency 40%, relative bandwidth 8%) and microwave band (conversion efficiency  $\approx 100\%$  and relative bandwidth 15%).<sup>[88]</sup> Nevertheless, transmission-type HWP with high efficiency is still absent at visible frequencies.

In contrast to the general predicament of low conversion efficiencies occurring to transmission-type wave plates, reflection-type counterparts could be readily realized with high efficiencies. Such polarization control capability has been accomplished by employing particle-insulator-metal configuration, which was initially proposed as a perfect absorber working at different frequency ranges.<sup>[93,94]</sup> Here, no transmission happened due to the optically thick metal substrate. Electromagnetic wave can be multiply reflected within the dielectric spacer, and sufficient phase delay accumulates to fulfill the phase requirement of either QWP or HWP.<sup>[16,83,90,95]</sup> Meanwhile, the inherent dispersion of resonant mode originating from top particles could be well neutralized by the thickness-dependent dispersion of dielectric spacer. A dispersion-less polarization control can thus be expected.<sup>[90]</sup> This structure was used to realize a HWP with polarization conversion efficiency close to 100% at the NIR range within a broad bandwidth, where the top material was silicon and the bottom substrate was silver (Figure 3d).<sup>[16]</sup> Because of the relatively low index contrast of the dielectric unit cell (compared with metal resonators), the thickness of the Si resonator is relatively large which may challenge to fabricate. Additionally, high efficiency is a result of sacrificing transmission property which causes limitations in many applications. So far, reflection-type designs with dielectric layer have been experimentally demonstrated to be the best way of enhancing the manipulation efficiency. Similar mechanism is also applicable to replace dielectric particles with metal counterparts.<sup>[83,89,90]</sup> For example, both QWP and HWP have been demonstrated with a high efficiency ( $>80\%$ ) covering a very broad band from 640 to 1300 nm, where both top and bottom materials were gold.<sup>[96]</sup>

Besides the polarization state conversion, it is also desired to arbitrarily rotate the polarization angle of linearly polarized light, which is usually required in types of situations, for instance, optical isolator, total internal reflection, and any other polarization dependent phenomena and devices. To overcome the bulk size of conventional polarization rotator based on either anisotropic or chiral materials, many artificial

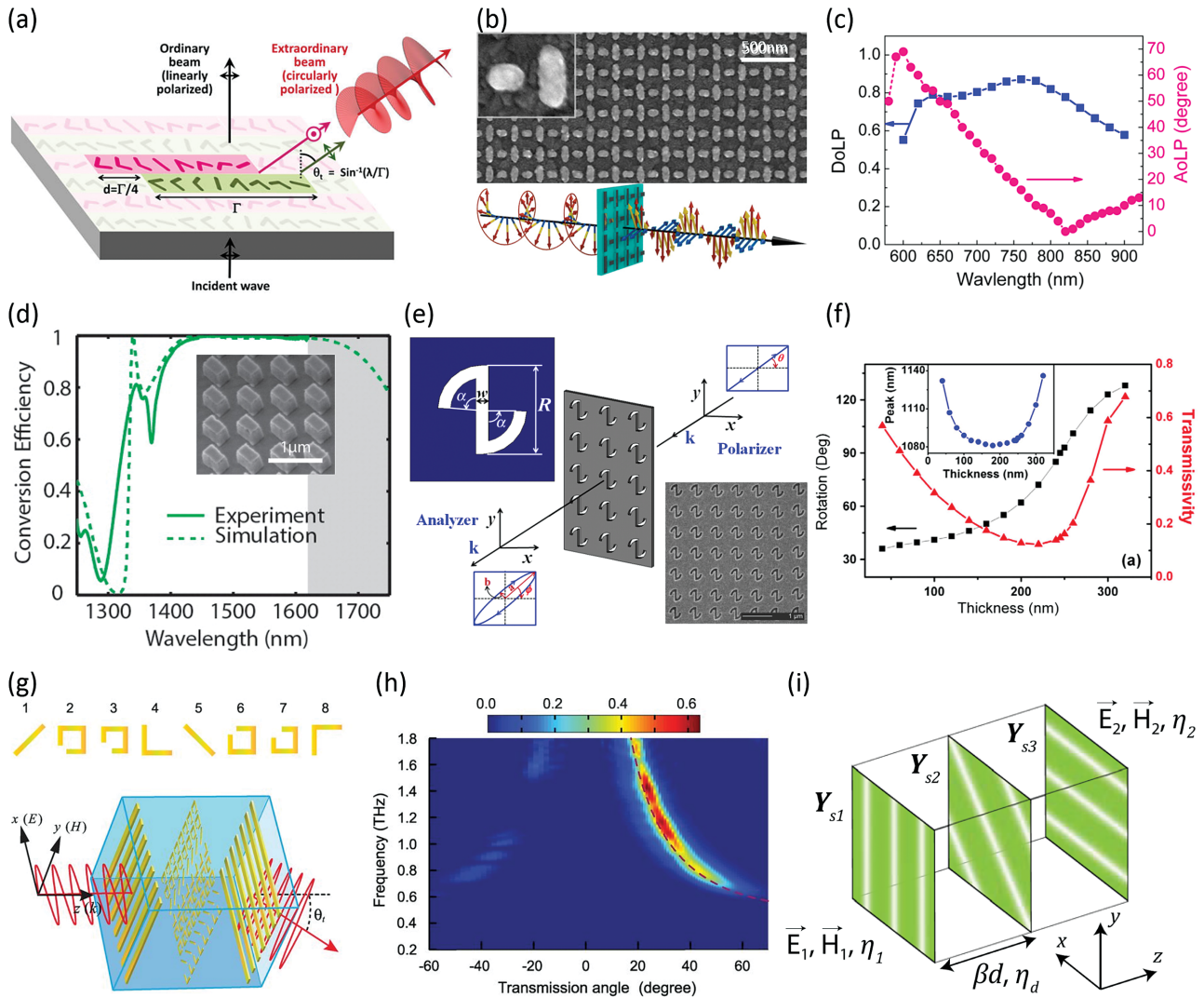


**Figure 3.** Polarizations control with metasurfaces. a) A broadband, background-free QWP realized with V-shaped nanoantenna array. Reproduced with permission.<sup>[14]</sup> Copyright 2012, ACS. b) Broadband polarization tailoring for visible light and c) experimentally measured degree of linear polarization (DoLP) and angle linear polarization (AoLP) for CP excitation. Reproduced with permission.<sup>[15]</sup> Copyright 2013, ACS. d) Half-wave plate realized with dielectric reflectarray. Reproduced with permission.<sup>[16]</sup> Copyright 2014, ACS. e) Polarization rotator based on coupling of waveguide mode and plasmonic mode and f) its performance. Reproduced with permission.<sup>[100]</sup> Copyright 2013, APS. g) Linear polarization conversion and anomalous refraction at terahertz frequencies and h) its experimental conversion efficiency as a function of frequency and angle. Reproduced with permission.<sup>[101]</sup> Copyright 2013, AAAS. i) Schematic of polarization control (rotator, polarizer, etc.) based on Huygens' metasurfaces. Reproduced with permission.<sup>[58]</sup> Copyright 2014, APS.

planar designs have been widely investigated.<sup>[91,97–99]</sup> However, either small rotation angle or moderate rotation efficiency has long awaited practical solutions. Figure 3e shows one type of polarization rotator based on coupling of waveguide mode and plasmonic mode.<sup>[100]</sup> By combining the contribution of both the LSPR and surface plasmons polaritons (SPPs), arbitrary rotation angle has been accomplished by simply modulating the thickness of the S-shaped through apertures in silver film. Particularly, a near-complete rotation (90°) at wavelength 1089 nm was obtained at a 245-nm-thickness silver film (Figure 3f). Nevertheless, due to the resonance origin, the operation bandwidth is usually very narrow. On the other hand, polarization control at terahertz frequencies is particularly fascinating due to the lack of suitable natural materials. As shown in Figure 3g,

a three-layer configurations was employed to achieve the polarization rotation with efficiency larger than 50% over a relative bandwidth 40%.<sup>[101]</sup> Especially, due to the introduction of a phase gradient at the middle layer, the rotated wave propagates at a deflected angle, similar to the achievement shown in Figure 3a. Recently, by cascading Huygens' anisotropic metasurfaces with judiciously selected admittances, exotic polarization conversions have also been accomplished (Figure 3i).<sup>[58]</sup>

Apart from polarization control, determination of polarization state is also significant for many applications. However, multiple measurements are usually needed to determine the Stokes parameters, which describe the polarization state with four parameters.<sup>[1,102,103]</sup> The setup is complex requiring several polarizers and wave plates since the four parameters are

calculated by intensities of two electric components in three different bases: the standard Cartesian base ( $\hat{x}, \hat{y}$ ), a Cartesian base rotated by  $45^\circ$  ( $\hat{a}, \hat{b}$ ) and a circular base ( $\hat{r}, \hat{i}$ ). Metasurfaces provide an effective way to reduce the complexity of detection process.<sup>[104–106]</sup> Through calculating the relative intensities, the ellipticity and handedness of a completely polarized incidence can be deduced based on PB-phase-enabled metasurface.<sup>[104]</sup> Furthermore, by judiciously integrate three sub-metasurfaces into one meta-grating, with which the power of an incident light with arbitrary polarization state will be diffracts six different directions. The Stokes parameters will then be calculated after one-step measurement.<sup>[105]</sup> As such, metasurfaces could also be employed to detect other parameters of EM waves, for example, the orbital angular momentum (OAM).<sup>[107,108]</sup>

### 3.3. Metahologram

Holography was first proposed in 1948 by Gabor to reconstruct the 3D imaging of an object by scattering an incident laser beam from the hologram, an optically recorded interference pattern.<sup>[109]</sup> Since then, it got a rapid development in many applications such as wavefront shaping and optical manipulation with the help of the CGHs,<sup>[110]</sup> which have been realized by the representative relief elements with propagation-accumulated phase,<sup>[111]</sup> and spatial light modulators (SLMs)<sup>[112]</sup> with reconfigurable and tunable functionalities. However, the relief elements seem incapable of tackling color holography well.<sup>[111]</sup> Worse still, with the limitations on fabrication technologies, their smallest achievable pixel size is as large as several micrometers (tens of wavelengths for visible light), which makes them not only suffer from high-order diffraction and twin-image issues, but also be incompetent at manipulating the polarization of visible light. Therefore, although metasurfaces allow the full manipulation of light, their most significant contribution to holography community is tailoring the polarization of light. To emphasize their significances, metasurface-based holograms are here classified in terms of polarization response: linear polarization and circular polarization metaholograms.

#### 3.3.1. Metaholograms for Linear Polarizations

Usually, either  $2\pi$ -phase and quasi-uniform amplitude modulation (Figure 3a) or pure-amplitude modulation (Figure 3b)<sup>[113,114]</sup> is required to reconstruct a holographic image through deliberately optimizing structure geometry for a linearly polarized light at one single wavelength. Due to the strong dispersion of plasmonic resonances, the response of phase and amplitude of a single structure is dispersive. Particularly, when the building structures support broad bandwidth resonances, this type of meta-hologram is able to render one image with variant colors.<sup>[51]</sup> However, in order to achieve a real multicolor meta-hologram, i.e., each image rebuilt with one single color, the selected structures have to be resonant at separated wavelengths. One effective approach is to form a super unit cell by combining multiple structures, which are resonant at totally different wavelengths (Figures 3c,d).<sup>[115,116]</sup> Different holographic images are reconstructed by addressing the incident

wavelengths, which works as a new metasurface-based wavelength-multiplexing technique. However, it should be noted that, in order to circumvent cross-talk of different wavelengths by spectrally separating employed resonances, the trade-off between color and phase/amplitude control inevitably results in low energy utilization efficiency for holographic images reconstruction.

Furthermore, by adopting the polarization response of biaxial two orthogonally orientated nanorods with large ratio of length to width to form a single pixel, polarization-dependent phase/amplitude response enables anisotropic response, i.e., two images can be encoded within one design (Figures 3e,f).<sup>[51,117]</sup> Alternatively, by using vectorial diffraction theory,<sup>[118,119]</sup> the isotropic refractive-index modulation structures have also shown polarization-multiplexed phase holograms (Figure 3g).<sup>[120]</sup>

Nevertheless, both wavelength and polarization multiplexing meta-holograms have low efficiency because of either low filling factor or small scattering cross section of nanostructures, as well as high ohmic loss of metals.<sup>[18,19,121]</sup> The highest efficiency for linear-polarization plasmonic meta-hologram is around 50% which it has just been achieved in a reflective operating mode at a NIR wavelength of 1550 nm.<sup>[122]</sup> In comparison, the dielectric meta-hologram with much lower absorption than metal can enhance the efficiency up to 91% at a wavelength of 915 nm in a transmission mode with the help of Mie scattering (Figure 3h).<sup>[17]</sup> Unfortunately, the high-efficiency (>80%) meta-hologram for linear polarization is not yet reported at the visible range thus far.

#### 3.3.2. Metaholograms for Circular Polarizations

Different from meta-holograms for linear polarizations, which are mainly achieved with geometry-dependent resonance response, metaholograms for circular polarizations gain the required phase control via orientation-rotated structures, i.e., PB phase. Due to the linear dependence of phase delay on orientation angle of individual structures, the engineering realization of multilevel phase for 3D holography<sup>[19]</sup> and holographic space-multiplexing (Figure 3i) are greatly simplified.<sup>[123]</sup> Remarkably, a reflection-type hologram with high efficiency beyond 80% has achieved based on this mechanism by using MIM structures.<sup>[20]</sup> It has also been developed to show circular-polarization dependent high-quality images efficiently in a broad bandwidth (Figure 4k),<sup>[46]</sup> making the metahologram more suitable for practical applications.

It is worthy to point out that the geometric phase based metasurface is dispersion free, which gives rise to a fail in wavelength multiplexing. In turn, the dispersion-less property makes these meta-holograms be able to operate at a broadband, i.e., displaying the same image with different colors.<sup>[19,20,46]</sup> All the reported meta-holograms designed for circular-polarization have no high-order diffraction and twin-image issues, being suffered by some linear-polarization meta-holograms,<sup>[51,113,115–117,122,124]</sup> because their effective pitches composed of arrayed nanostructures have the wavelength-scale (i.e., larger than one wavelength) size. Genevet et al. have a more detailed discussion on meta-hologram and applications based on holographic metasurfaces.<sup>[125]</sup>

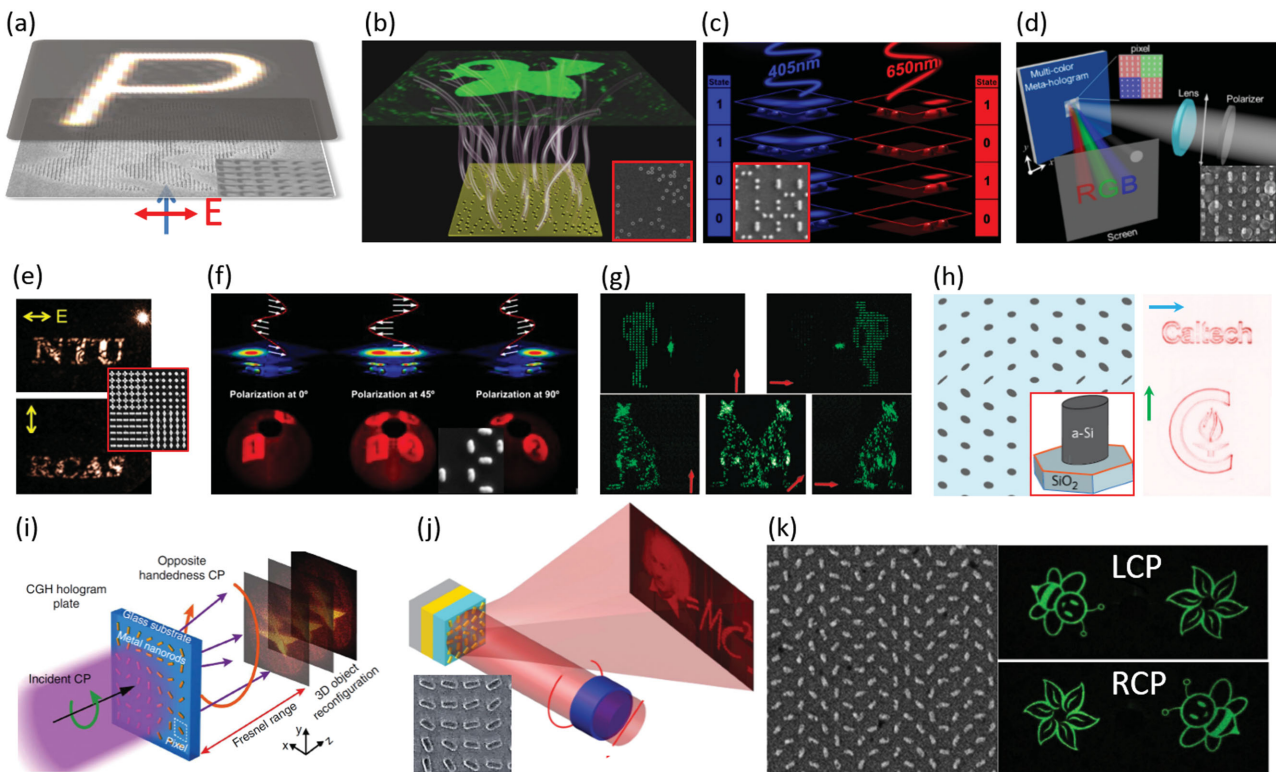


**Figure 4.** Hologram realized with metasurfaces. a) Metasurface holography for linear polarization realized by V-shaped nanoapertures. Reproduced with permission.<sup>[18]</sup> Copyright 2013, NPG. b) Nanosieve hologram. Reproduced with permission.<sup>[114]</sup> Copyright 2015, NPG. c) Two-color metahologram realized by nanoparticle scatters.<sup>[115]</sup> d) Color metahologram realized by rectangle nanorods. Reproduced with permission.<sup>[95]</sup> Copyright 2015, ACS. e–g) Polarization-multiplexing metaholograms. Arrows represents the polarization of electric field. e) Reproduced with permissions.<sup>[51]</sup> Copyright 2013, ACS. f) Reproduced with permission.<sup>[117]</sup> Copyright 2014, ACS. g) Reproduced with permission.<sup>[120]</sup> Copyright 2015, NPG. h) High efficiency silicon metaholograms. Reproduced with permission.<sup>[17]</sup> Copyright 2015, NPG. i) Metahologram based on PB phase. Reproduced with permission. Copyrights 2013, NPG. j) Metahologram based on hybrid of PB phase and MIM structures. Reproduced with permission. Copyright 2015, NPG. k) Helicity multiplexed metaholograms. i) Reproduced with permission.<sup>[19]</sup> Copyright 2013, NPG. j) Reproduced with permission.<sup>[20]</sup> Copyright 2015, NPG. k) Reproduced with permission.<sup>[46]</sup> Copyright 2015, NPG.

### 3.4. Angular Momentum of EM Waves

The mechanical properties of light have intrigued a myriad of applications such as optical trapping,<sup>[126]</sup> optical communication<sup>[127,128]</sup> and microscopy.<sup>[129,130]</sup> Besides linear momentum, light can also carry angular momentum, i.e., spin and orbital angular momenta.<sup>[131]</sup> Spin angular momentum (SAM) of light was first realized in 1909 by Poynting, which was associated with the circular polarization.<sup>[132–134]</sup> However, the OAM of light was recognized until 1992, which was carried by an azimuthal phase dependence of  $\exp(-il\phi)$  and independent of the polarization state. Here  $l$  is the topological charge, indicating the number of twists of the wavefront within one wavelength.<sup>[135,136]</sup> Till now, various methods have been proposed to generate vortex beam with different topological charges, such as spiral phase plates,<sup>[137]</sup> SLM,<sup>[138]</sup> Q-plate,<sup>[139]</sup> cylindrical mode converters.<sup>[140]</sup> However, these bulk elements impose the great challenges on their integration with other optical devices, however, which can be feasibly overcome with the metasurfaces.

By arranging eight constitute antennas to form an azimuthal phase delay ranging from 0 to  $2\pi$  (Figure 5a), a spiral-like phase delay will be imparted to the planar wavefront of the incident wave (Figure 5b).<sup>[7]</sup> Here the topological

charge is 1. Its feature can be identified by interfering with a normal spherical wave or inclined plane wave. Such beam wavefront can also be achieved for CP light by using PB phase.<sup>[9]</sup> Alternatively, hologram has been used as an effective approach to generate spiral phase. As an example, by fabricated structures with fork patterns (Figure 5c), the corresponding spiral phase can be created by using Gaussian beam as an incidence.<sup>[141]</sup> Meanwhile, the radially polarized beam (RPB), which is filtered out by subwavelength ring-shaped radial polarizer, inevitably carries unwanted spatially varying phase distributions ( $e^{i\theta}$ ). As a result, the superposition of the radial polarizer and the fork diffraction hologram can generate phase compensated radially polarized light. To be more specific, the RPB is selected by the subwavelength apertures, and the deviated PB phase was compensated by spiral phase of the  $-1$  order beam generated by the fork hologram. As shown in Figure 5d, it is obvious that different polarization states can be well selected by a linear polarizer. Notably, the working wavelength covers the long end of visible range with a relative bandwidth 30%.

Besides the generation of OAM, efficient detection of vortex beam is also significant for exploiting its potentials. However, different topological charges are hard to be selectively detected

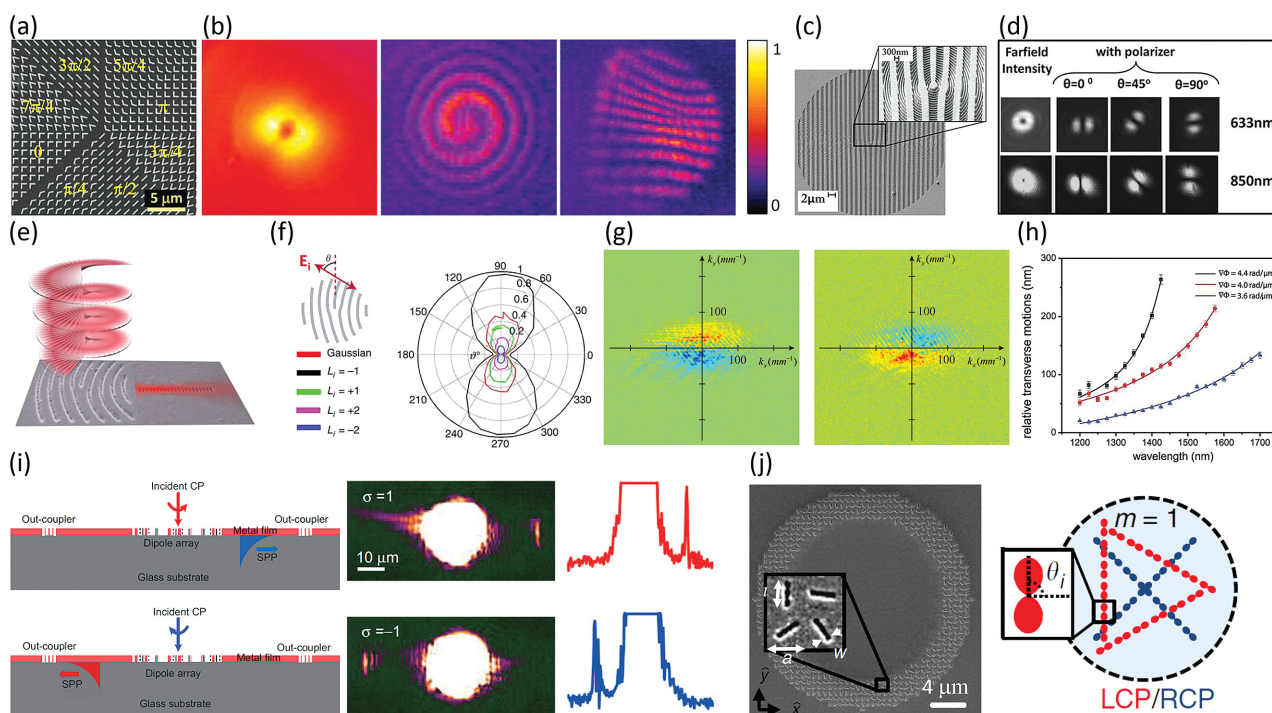


**Figure 5.** Vortex beam generation, detection, and spin-orbital interaction enhancement based on metasurfaces. a) OAM generation with V-shaped nanoantennas and b) far-field intensity distribution of an optical vortex with topological charge 1 (left), spiral patterns (middle), and dislocated fringe (right) are created by the on-axis and off-axis interference of the vortex beam and a Gaussian beam, respectively. a,b) Reproduced with permission.<sup>[7]</sup> Copyright 2011, AAAS c) A plasmonic detour-phase hologram filled with nanoscale apertures is able to manipulate phase, amplitude and polarization simultaneously. d) A radially polarized beam is generated and far-field intensity distributions are filtered by an analyzer oriented along different angles. c,d) Reproduced with permission.<sup>[141]</sup> Copyright 2013, ACS. e) A holographic interface consisting of curved, fork-shaped grooves couples an incident vortex beam with topological charge -1 into a focused surface wave and f) detected photocurrent as a function of the incident polarization and topological charge. The inset shows the orientation of the polarization of the incident electric field with respect to the grooves. e,f) Reproduced with permission.<sup>[107]</sup> Copyright 2012, NPG. g) Observation of giant OSHE with incident light polarized along x- (left) and y- (right) axes. Red and blue represent the right and left CP lights, respectively. h) Relative transverse motion between anomalously refracted light beams with right CP and left CP lights. g,h) Reproduced with permission.<sup>[144]</sup> Copyright 2013, AAAS. i) Spin selective unidirectional SPP wave based on PB phase metasurface. Working principle (left) and experimental demonstrations (middle and right). Reproduced with permission.<sup>[145]</sup> Copyright 2013, NPG. j) Spin-dependent light control. Left: top-view SEM image of experiment sample. Right: arbitrary spin-dependent SPP profiles with more complicated pattern. Reproduced with permission.<sup>[149]</sup> Copyright 2015, NPG.

since such information is carried by the azimuthal phase, which is impossible to be recorded with conventional photo-detectors. Inspired by the principle of hologram, efficient OAM sorting techniques have been developed by using diffractive optical elements to convert OAM states into transverse momentum states.<sup>[142,143]</sup> In order to fulfil the conservation of angular momentum, an opposite OAM is required to impart to the incident vortex beam. As shown in Figure 5e, a hologram consisting of fork-like nanostructures was patterned on the metal film being able to convert an incoming vortex beam with topological charge  $l = -1$  to a focused SPPs without OAM.<sup>[107]</sup> The detected results of incident light with different OAM are presented in Figure 5f. In the shown example, due to the on-purpose design, the complex coupler can selectively couple vortex beam with given topological charge by compensating the phase via scattering. Detection of higher order OAM can also be achieved with good selectivity by modifying the holographic coupler. By using multiple plasmonic semi-ring slits, another simpler method was also able to sort OAM, which was based on the constructive interference of a phase-modulated SPPs at a wavelength 633 nm.<sup>[108]</sup>

Optical spin Hall effect (OSHE) has significant potentials in optical communications and information processing. However, extremely small photon momentum and weak spin-orbit interaction make it hard to be observed. As light propagating in homogeneous media, both spin and orbital angular momenta are independent on each other. But, in a complex medium or inhomogeneous medium, they will interact with each other.<sup>[139]</sup> Momentum exchange leads to changes in polarization and propagation trajectory. Unlike previous designs with multiple reflections or ultrasensitive quantum weak measurements with pre- and post-selections of spin state, plasmonic metasurfaces allows the direct observation of large transverse motion of CP light through breaking the axial symmetry of the system. As shown in Figure 5g, by using V-shaped nanostructures, positions-dependent phase discontinuity breaks the axial symmetry of the system and allow strong spin-orbital coupling.<sup>[144]</sup> A relative transverse shift can be readily measured. Although the shift amount could be increased by introducing a larger in-plane phase gradient, it may be still too small to be used in practice (Figure 5h). Metasurfaces based on PB phase provide another excellent strategy to realize helicity-dependent wave

propagation.<sup>[145,146]</sup> Because of the interfacial phase discontinuity generated by PB phase metasurfaces, the incident beam will be added additional linear momentum with the sign determined by its helicity. As a result, incident beams with opposite helicities will be guided into different directions following the equation below:<sup>[145]</sup>

$$n_t \sin \theta_t = \frac{\lambda_0}{p} \left( m + 2\sigma \frac{\Delta\varphi}{2\pi} \right) \quad (2)$$

where  $n_t$  and  $\theta_t$  are the refractive index and angle for the transmitted light, respectively.  $\lambda_0$  is the incident wavelength in vacuum and  $\sigma$  represents the helicity of the incident beam, which takes the values of  $\pm 1$ .  $m$  is the diffraction order and  $p$  is the periodicity of unit cells. More importantly, by matching Equation (2), the emergent light could be either surface wave (Figure 5i) or propagating wave.<sup>[145,146]</sup> However, current practices are usually achieved with low efficiency because of undesired zeroth order reflection and transmission. Relatively, such unwanted scattering could be easily eliminated in reflection-type designs by blocking the transmission with an optically thickness substrate, as in MIM systems. By further satisfying the condition  $r_{uu} + r_{vv} = r_{uu} - r_{vv} = 0$ , the OSHE was demonstrated with nearly 100% efficiency, where  $r_{ij}$  ( $i$  and  $j = u$  and  $v$ ) are the reflection coefficients defined in the Cartesian coordinate system with two axes  $\hat{u}$  and  $\hat{v}$ .<sup>[147]</sup>

Nonetheless, generic metasurfaces based on PB phase have a vital defect that the achieved functionalities in controlling EM waves are usually symmetric for two opposite spins, such as focusing/defocusing, left/right and inward/outward.<sup>[41,44,46,145–148]</sup> In principle, each PB phase element (for example, nanorod and nanoslot) acts as a dipole source. To reconstruct a target field distribution, we need to ensure a constructive interference of radiations from different elements, whose spatial distributions are determined by  $\theta(x, y) = f_{\pm}(E_z) = \pm \arg(\partial_x E_z \pm i \partial_y E_z) / 2 + \text{const.}$ , where  $E_z$  is the target field and  $\pm$  is associated with two spins. Due to the opposite signs of induced phases, the propagation behavior will be opposite as well for two spins. Consequently, the manipulation is far from arbitrary and independent. It is lately realized that such undesired symmetry could be removed when the target field profile within a specific region is replaced with a superposition of two or multiple target fields. As shown in Figure 5j, a ring consisting of nanoslots was used to demonstrate spin-dependent SPP wave control in an arbitrary way.<sup>[149]</sup>

### 3.5. Other Applications

Novel functionalities of metasurfaces continue to be explored benefiting from their full capabilities in controlling EM waves. One of most important applications of metamaterials is cloaking devices, with which objects can be hidden from the incoming waves. It was numerically proved that, by compensating the local phases with graded metasurfaces, a unidirectional carpet cloak is achievable to mimic the reflection from a flat ground, with which an arbitrary object can be hidden in the prescribed region.<sup>[150–153]</sup> Freshly, an ultrathin invisibility skin cloak for visible light was realized experimentally by spatially distributing

the MIM-type resonators (Figure 6a).<sup>[154]</sup> In comparison of bulky cloaks realized via 3D metamaterials, the achieved metasurface cloak was only with thickness 80 nm (one ninth of the operation wavelength). Due to the scalable feature of EM response, it is thus expectable that metasurface-based cloak can be readily extended to macroscopic sizes. In addition, the metasurface-based cloaks are more straightforward and practicable since there is no complex materials parameter involved.

Optical pulling force attracted a great deal of interest due to their fascinating feasibility for micromanipulation.<sup>[155–157]</sup> Propagation-invariant Bessel beam is one of the particular candidates to generate an ambient-independent pulling force. Lately, such force was theoretically gained via a dielectric metasurface (Figure 6b). The proposed Si metasurface was able to convert a normally incident Gaussian beam into a tractor beam over a distance of  $5\lambda_0$ , where  $\lambda_0$  is the operation wavelength.<sup>[158]</sup> The manipulation region can be further enlarged by increasing the diameter of metasurface and Gaussian beam. It opens a remarkable door to generate other structured beams to realize more sophisticated particle manipulations in diverse environments.<sup>[159–162]</sup>

Different achievements contribute immensely towards the growth of metasurfaces. Some fascinating stories continue to be put on the stage, such as 2D analogue of Cherenkov radiation (Figure 6c),<sup>[163]</sup> mathematical operation (Figure 6d),<sup>[164,165]</sup> nonlinear metasurface (Figure 6e)<sup>[166]</sup> and remote quantum interference (Figure 6f).<sup>[167]</sup> Beside the spatial gradient, a transverse temporal gradient can also be taken into account to break the reciprocity symmetry, which shows important application in nonreciprocal devices, such as optical diode.<sup>[168]</sup> More comprehensively, such concept of wave control has been applied to diverse disciplines for wave-matter interactions, such as acoustics,<sup>[169,170]</sup> thermal physics,<sup>[171,172]</sup> etc.

## 4. Conclusions and Outlook

In this review, the recent advances—from the past few years—in metasurface-based applications have been presented from the perspective of achieved functionalities. Metasurfaces become one of the most promising candidates to replace conventional EM elements, being more applicable to miniaturized photoelectric devices with high integrity. As one of the key performance factors, the manipulation efficiencies of existing metasurfaces have to be improved further, especially for transmission-type manipulation at visible frequencies (Table 1). The low efficiency issues seem being solved by semiconductors or high-index dielectrics due to their smaller intrinsic losses at longer wavelengths. Especially silicon metasurfaces are more compatible with the established semiconductor processing technologies. At visible frequencies, there is still a long way to go.

Nevertheless, most of the existing metasurface-based demonstrations show a lack of tunability. In order to achieve an active metasurface, the material properties of either building structures or the dielectric environment have to be tunable. Both approaches result from the material-dependent resonance responses. The latter approach has been extensively used for sensing applications. Providentially, various of materials are lined up for active device designs, such as phase change

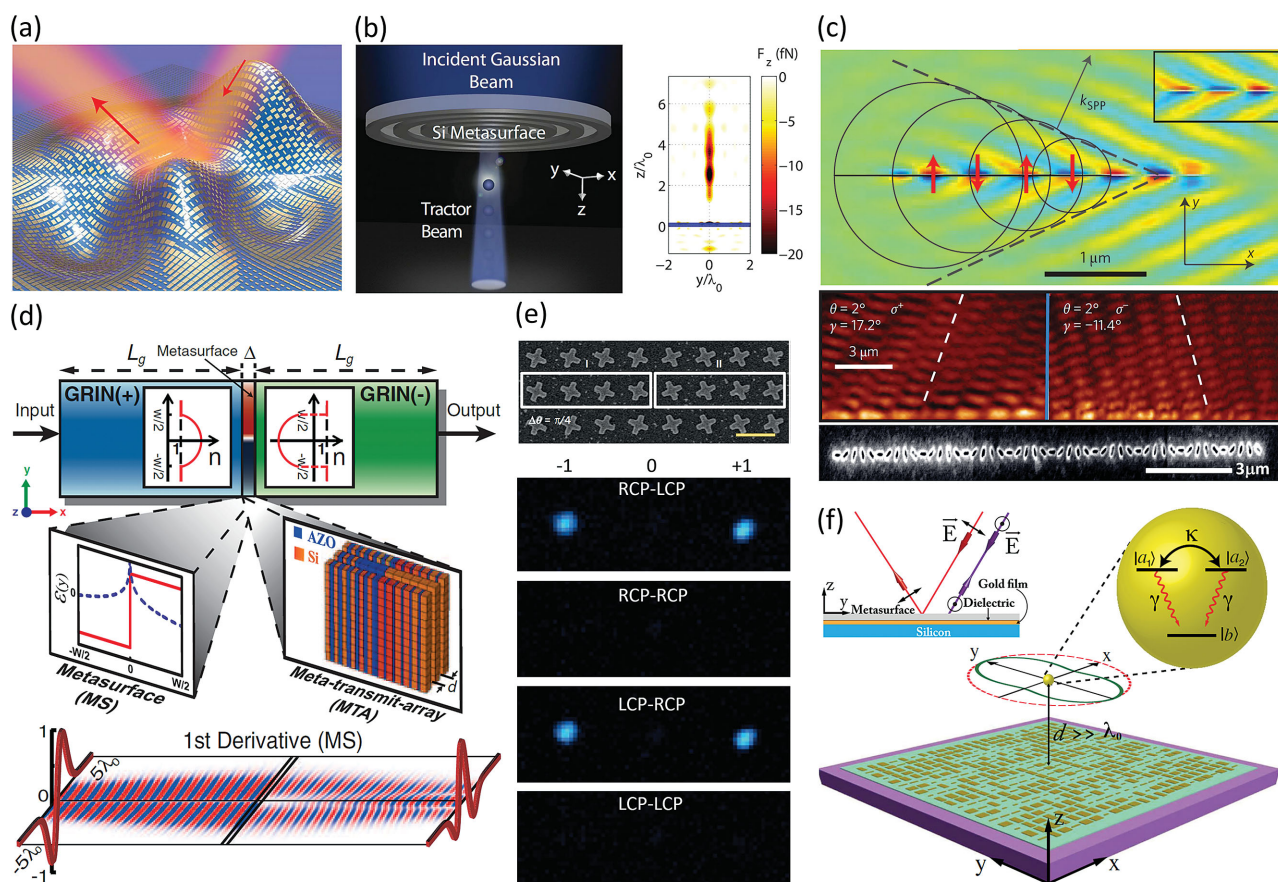


**Figure 6.** Other applications of metasurfaces. a) Metasurface cloak for visible light. Reproduced with permission.<sup>[154]</sup> Copyright 2015, AAAS. b) Generating stable tractor beams with dielectric metasurfaces. Reproduced with permission.<sup>[158]</sup> Copyright 2015, APS. c) Cherenkov surface plasmon wakes with one-dimensional metamaterials. Reproduced with permission.<sup>[163]</sup> Copyright 2015, NPG. d) Mathematical operation with metasurfaces. Reproduced with permission.<sup>[164]</sup> Copyright 2014, AAAS. e) Anomalous light control with nonlinear metasurfaces. Reproduced with permission.<sup>[166]</sup> Copyright 2015, NPG. f) Metasurface-enabled remote quantum interference. Reproduced with permission.<sup>[167]</sup> Copyright 2015, APS.

materials (PCMs),<sup>[173–178]</sup> 2D materials,<sup>[179,180]</sup> liquid crystals,<sup>[181]</sup> microelectromechanical systems (MEMS)<sup>[182,183]</sup> and PIN diodes.<sup>[184]</sup> The tunable performance can be accomplished via optical, electrical, or mechanical approaches by selecting

appropriate active materials. For instance, an active polarizer was demonstrated at millimeter range. By switching on/off each PIN diode individually, the system can either convert the linearly polarized light into right CP or left CP light, while it

**Table 1.** Comparison of experimental manipulation efficiencies at visible range.

Functionality	Type	Building block	Efficiency <sup>a)</sup>	Wavelength	Material <sup>b)</sup>
Bending	Reflection	Gap mode	80%	850 nm	Gold <sup>[9]</sup>
	Transmission	PB phase	20%	550 nm	Poly-Si <sup>[70]</sup>
Focusing	Reflection	Gap mode	14–27%	750–950 nm	Gold <sup>[80]</sup>
	Transmission	PB phase	15%	633 nm	Ag <sup>[81]</sup>
Quarter wave plate	Reflection	Gap mode	84%	640–1330 nm	Gold <sup>[96]</sup>
	Transmission	Cross coupling <sup>c)</sup>	50%	615–835 nm	Silver <sup>[15]</sup>
Half wave plate	Reflection	Gap mode	85%	640–1400 nm	Gold <sup>[96]</sup>
	Transmission	Cross coupling <sup>c)</sup>	10%	800 nm	Gold <sup>[88]</sup>
Hologram	Reflection	PB phase & gap mode	80%	600–1000 nm	Gold <sup>[20]</sup>
	Transmission	Hybrid mode	10%	676 nm	Gold <sup>[18]</sup>

<sup>a)</sup>Efficiency: defined as the fraction of the incident energy that contributes to the part being manipulated; <sup>b)</sup>Material refers to the main part in metasurface system which supports the resonance. Substrate and dielectric spacer are not listed; <sup>c)</sup>Cross coupling indicates a strong polarization conversion based on two orthogonal nanorods or nanoslots.

can also be isotropic to retain the incident polarization at millimeter wave.<sup>[184]</sup>

As one of the most important optical topics, nonlinear effects have been well developed after the invention of the laser technology.<sup>[185]</sup> Lately, it has also been taken into account to design metasurface-based deflectors.<sup>[166]</sup> With the up- or downconversion nonlinear effect, more exciting functionalities will be realized in the years to come. One can find more discussion on nonlinear metasurfaces elsewhere.<sup>[23,26]</sup> In addition, from the perspective of practical applications, metasurfaces fabricated on flexible substrate possess broad application prospects.<sup>[186,187]</sup>

Although metasurfaces underwent a rapid development in the past few years, there is still a long way to go to find a satisfactory and complete solutions for several issues such as the high-efficiency transmission type applications for visible and even ultraviolet light and tunability. In the expectable future, more efforts are going to be attracted to bring metasurfaces from laboratory scale to practical applications, which will contribute towards more favorable optical elements with ultracompact size, multiple functionalities, high integrity, etc.

## Acknowledgements

L.Z. and C.-W. Q. would like to acknowledge financial support by the National University of Singapore (Grant No. R-263-000-A45-112). C.-W.Q. would like to acknowledge the support by A\*STAR BEP project (Grant No. R-263-000-B88-305), via the administration of National University of Singapore. K.H. would like to acknowledge the financial support by A\*STAR BEP project (Grant No. IMRE/15-2C0308), Singapore.

Received: November 24, 2015

Revised: January 17, 2016

Published online: March 4, 2016

- [1] M. Born, E. Wolf, *Principles of Optics*, Cambridge University Press, Cambridge, UK 1999.
- [2] J. B. Pendry, *Phys. Rev. Lett.* **2000**, *85*, 3966.
- [3] H. Chen, B. Hou, S. Chen, X. Ao, W. Wen, C. T. Chan, *Phys. Rev. Lett.* **2009**, *102*, 183903.
- [4] J. B. Pendry, D. Schurig, D. R. Smith, *Science* **2006**, *312*, 1780.
- [5] D. Schurig, J. J. Mock, B. J. Justice, S. A. Cummer, J. B. Pendry, A. F. Starr, D. R. Smith, *Science* **2006**, *314*, 977.
- [6] B. A. Munk, *Frequency Selective Surfaces: Theory and Design*, John Wiley, New York 2000.
- [7] N. Yu, P. Genevet, M. A. Kats, F. Aieta, J.-P. Tetienne, F. Capasso, Z. Gaburro, *Science* **2011**, *334*, 333.
- [8] X. Ni, N. K. Emani, A. V. Kildishev, A. Boltasseva, V. M. Shalaev, *Science* **2012**, *335*, 427.
- [9] L. Huang, X. Chen, H. Mühlenbernd, G. Li, B. Bai, Q. Tan, G. Jin, T. Zentgraf, S. Zhang, *Nano Lett.* **2012**, *12*, 5750.
- [10] S. Sun, K.-Y. Yang, C.-M. Wang, T.-K. Juan, W. T. Chen, C. Y. Liao, Q. He, S. Xiao, W.-T. Kung, G.-Y. Guo, L. Zhou, D. P. Tsai, *Nano Lett.* **2012**, *12*, 6223.
- [11] Y. F. Yu, A. Y. Zhu, R. Paniagua-Domínguez, Y. H. Fu, B. Luk'yanchuk, A. I. Kuznetsov, *Laser Photonics Rev.* **2015**, *9*, 412.
- [12] F. Aieta, P. Genevet, M. A. Kats, N. Yu, R. Blanchard, Z. Gaburro, F. Capasso, *Nano Lett.* **2012**, *12*, 4932.
- [13] A. Pors, M. G. Nielsen, R. L. Eriksen, S. I. Bozhevolnyi, *Nano Lett.* **2013**, *13*, 829.
- [14] N. Yu, F. Aieta, P. Genevet, M. A. Kats, Z. Gaburro, F. Capasso, *Nano Lett.* **2012**, *12*, 6328.
- [15] Y. Zhao, A. Alù, *Nano Lett.* **2013**, *13*, 1086.
- [16] Y. Yang, W. Wang, P. Moitra, I. I. Kravchenko, D. P. Briggs, J. Valentine, *Nano Lett.* **2014**, *14*, 1394.
- [17] A. Arbabi, Y. Horie, M. Bagheri, A. Faraon, *Nat. Nanotechnol.* **2015**, *10*, 937.
- [18] X. Ni, A. V. Kildishev, V. M. Shalaev, *Nat. Commun.* **2013**, *4*, 3807.
- [19] L. Huang, X. Chen, H. Mühlenbernd, H. Zhang, S. Chen, B. Bai, Q. Tan, G. Jin, K.-W. Cheah, C.-W. Qiu, J. Li, T. Zentgraf, S. Zhang, *Nat. Commun.* **2013**, *4*, 3808.
- [20] G. Zheng, H. Mühlenbernd, M. Kenney, G. Li, T. Zentgraf, S. Zhang, *Nat. Nanotechnol.* **2015**, *10*, 308.
- [21] S. A. Maier, *Plasmonics: Fundamentals and Applications*, SpringerUS, New York 2007.
- [22] B. Luk'yanchuk, N. I. Zheludev, S. A. Maier, N. J. Halas, P. Nordlander, H. Giessen, C. T. Chong, *Nat. Mater.* **2010**, *9*, 707.
- [23] M. Kauranen, A. V. Zayats, *Nat. Photonics* **2012**, *6*, 737.
- [24] N. Yu, F. Capasso, *Nat. Mater.* **2014**, *13*, 139.
- [25] N. Meinzer, W. L. Barnes, I. R. Hooper, *Nat. Photonics* **2014**, *8*, 889.
- [26] A. E. Minovich, A. E. Miroshnichenko, A. Y. Bykov, T. V. Murzina, D. N. Neshev, Y. S. Kivshar, *Laser Photonics Rev.* **2015**, *9*, 195.
- [27] P. Ghenuche, S. Cherukulappurath, T. H. Taminiau, N. F. van Hulst, R. Quidant, *Phys. Rev. Lett.* **2008**, *101*, 116805.
- [28] L. Novotny, N. van Hulst, *Nat. Photonics* **2011**, *5*, 83.
- [29] N. Yu, P. Genevet, F. Aieta, M. A. Kats, R. Blanchard, G. Aoust, J. P. Tetienne, Z. Gaburro, F. Capasso, *IEEE J. Sel. Top. Quantum Electron.* **2013**, *19*, 4700423.
- [30] R. Blanchard, G. Aoust, P. Genevet, N. Yu, M. A. Kats, Z. Gaburro, F. Capasso, *Phys. Rev. B* **2012**, *85*, 155457.
- [31] M. A. Kats, P. Genevet, G. Aoust, N. Yu, R. Blanchard, F. Aieta, Z. Gaburro, F. Capasso, *Proc. Natl. Aca. Sci. USA* **2012**, *109*, 12364.
- [32] M. Kang, T. Feng, H.-T. Wang, J. Li, *Opt. Express* **2012**, *20*, 15882.
- [33] X. Ni, S. Ishii, A. V. Kildishev, V. M. Shalaev, *Light Sci. Appl.* **2013**, *2*, e72.
- [34] S. Pancharatnam, *Proc. Indian Acad. Sci.* **1956**, *44*, 247.
- [35] M. V. Berry, *J. Mod. Opt.* **1987**, *34*, 1401.
- [36] Z. e. Bomzon, V. Kleiner, E. Hasman, *Opt. Lett.* **2001**, *26*, 1424.
- [37] Z. e. Bomzon, G. Biener, V. Kleiner, E. Hasman, *Opt. Lett.* **2002**, *27*, 1141.
- [38] U. Levy, H.-C. Kim, C.-H. Tsai, Y. Fainman, *Opt. Lett.* **2005**, *30*, 2089.
- [39] L. Liu, X. Zhang, M. Kenney, X. Su, N. Xu, C. Ouyang, Y. Shi, J. Han, W. Zhang, S. Zhang, *Adv. Mater.* **2014**, *26*, 5031.
- [40] S.-C. Jiang, X. Xiong, Y.-S. Hu, S.-W. Jiang, Y.-H. Hu, D.-H. Xu, R.-W. Peng, M. Wang, *Phys. Rev. B* **2015**, *91*, 125421.
- [41] X. Ding, F. Monticone, K. Zhang, L. Zhang, D. Gao, S. N. Burokur, A. de Lustrac, Q. Wu, C.-W. Qiu, A. Alù, *Adv. Mater.* **2015**, *27*, 1195.
- [42] L. Cong, N. Xu, J. Han, W. Zhang, R. Singh, *Adv. Mater.* **2015**, *27*, 6630.
- [43] L. Cong, N. Xu, W. Zhang, R. Singh, *Adv. Opt. Mater.* **2015**, *3*, 11176.
- [44] X. Chen, L. Huang, H. Mühlenbernd, G. Li, B. Bai, Q. Tan, G. Jin, C.-W. Qiu, S. Zhang, T. Zentgraf, *Nat. Commun.* **2012**, *3*, 1198.
- [45] X. Chen, L. Huang, H. Mühlenbernd, G. Li, B. Bai, Q. Tan, G. Jin, C.-W. Qiu, T. Zentgraf, S. Zhang, *Adv. Opt. Mater.* **2013**, *1*, 517.
- [46] D. Wen, F. Yue, G. Li, G. Zheng, K. Chan, S. Chen, M. Chen, K. F. Li, P. W. H. Wong, K. W. Cheah, E. Yue Bun Pun, S. Zhang, X. Chen, *Nat. Commun.* **2015**, *6*, 8241.
- [47] D. Wen, S. Chen, F. Yue, K. Chan, M. Chen, M. Ardrón, K. F. Li, P. W. H. Wong, K. W. Cheah, E. Y. B. Pun, G. Li, S. Zhang, X. Chen, *Adv. Opt. Mater.* **2015**, DOI: 10.1002/adom.201500498.
- [48] F. Monticone, N. M. Estakhri, A. Alù, *Phys. Rev. Lett.* **2013**, *110*, 203903.
- [49] N. Liu, H. Guo, L. Fu, S. Kaiser, H. Schweizer, H. Giessen, *Adv. Mater.* **2007**, *19*, 3628.
- [50] A. Pors, O. Albrektsen, I. P. Radko, S. I. Bozhevolnyi, *Sci. Rep.* **2013**, *3*, 2155.

- [51] W. T. Chen, K.-Y. Yang, C.-M. Wang, Y.-W. Huang, G. Sun, I. D. Chiang, C. Y. Liao, W.-L. Hsu, H. T. Lin, S. Sun, L. Zhou, A. Q. Liu, D. P. Tsai, *Nano Lett.* **2013**, *14*, 225.
- [52] L. Zhang, J. Hao, H. Ye, S. P. Yeo, M. Qiu, S. Zouhdi, C.-W. Qiu, *Nanoscale* **2013**, *5*, 3373.
- [53] L. Zhang, J. Hao, M. Qiu, S. Zouhdi, J. K. W. Yang, C.-W. Qiu, *Nanoscale* **2014**, *6*, 12303.
- [54] A. E. H. Love, *Philos. Trans. R. Soc. London A: Math. Phys. Eng. Sci.* **1901**, 197, 1.
- [55] S. A. Schelkunoff, *AT&T Tech. J.* **1936**, *15*, 92.
- [56] C. Pfeiffer, A. Grbic, *Phys. Rev. Lett.* **2013**, *110*, 197401.
- [57] C. Pfeiffer, N. K. Emani, A. M. Shaltout, A. Boltasseva, V. M. Shalaev, A. Grbic, *Nano Lett.* **2014**, *14*, 2491.
- [58] C. Pfeiffer, A. Grbic, *Phys. Rev. Appl.* **2014**, *2*, 044011.
- [59] F. Qin, L. Ding, L. Zhang, F. Monticone, C. C. Chum, J. Deng, S. Mei, Y. Li, J. Teng, M. Hong, S. Zhang, A. Alù, C.-W. Qiu, *Sci. Adv.* **2015**, *2*, e1501168.
- [60] Y. Cui, J. Xu, K. H. Fung, Y. Jin, A. Kumar, S. He, N. X. Fang, *Appl. Phys. Lett.* **2011**, *99*, 253101.
- [61] Y. Cui, K. H. Fung, J. Xu, H. Ma, Y. Jin, S. He, N. X. Fang, *Nano Lett.* **2012**, *12*, 1443.
- [62] M. M. Hossain, B. Jia, M. Gu, *Adv. Opt. Mater.* **2015**, *3*, 1047.
- [63] Y. Z. Cheng, W. Withayachumnankul, A. Upadhyay, D. Headland, Y. Nie, R. Z. Gong, M. Bhaskaran, S. Sriram, D. Abbott, *Adv. Opt. Mater.* **2015**, *3*, 376.
- [64] Q. Liang, T. Wang, Z. Lu, Q. Sun, Y. Fu, W. Yu, *Adv. Opt. Mater.* **2013**, *1*, 43.
- [65] F. Aieta, M. A. Kats, P. Genevet, F. Capasso, *Science* **2015**, *347*, 1342.
- [66] M. Khorasaninejad, F. Aieta, P. Kanhaiya, M. A. Kats, P. Genevet, D. Rousso, F. Capasso, *Nano Lett.* **2015**, *15*, 5358.
- [67] C. F. H. Bohren, R. Donald, *Absorption and Scattering of Light by Small Particles*, Wiley-VCH, Weinheim, Germany **1983**.
- [68] L. Cao, J. S. White, J.-S. Park, J. A. Schuller, B. M. Clemens, M. L. Brongersma, *Nat. Mater.* **2009**, *8*, 643.
- [69] L. Cao, P. Fan, E. S. Barnard, A. M. Brown, M. L. Brongersma, *Nano Lett.* **2010**, *10*, 2649.
- [70] D. Lin, P. Fan, E. Hasman, M. L. Brongersma, *Science* **2014**, *345*, 298.
- [71] A. Arbabi, Y. Horie, A. J. Ball, M. Bagheri, A. Faraon, *Nat. Commun.* **2015**, *6*, 7069.
- [72] M. Decker, I. Staude, M. Falkner, J. Dominguez, D. N. Neshev, I. Brener, T. Pertsch, Y. S. Kivshar, *Adv. Opt. Mater.* **2015**, *3*, 813.
- [73] F. H. L. Koppens, D. E. Chang, F. J. García de Abajo, *Nano Lett.* **2011**, *11*, 3370.
- [74] Z. Fei, A. S. Rodin, G. O. Andreev, W. Bao, A. S. McLeod, M. Wagner, L. M. Zhang, Z. Zhao, M. Thieme, G. Dominguez, M. M. Fogler, A. H. C. Neto, C. N. Lau, F. Keilmann, D. N. Basov, *Nature* **2012**, *487*, 82.
- [75] V. W. Brar, M. S. Jang, M. Sherrott, J. J. Lopez, H. A. Atwater, *Nano Lett.* **2013**, *13*, 2541.
- [76] A. N. Grigorenko, M. Polini, K. S. Novoselov, *Nat. Photonics* **2012**, *6*, 749.
- [77] M. A. Dupertuis, B. Acklin, M. Proctor, *J. Opt. Soc. Am. A* **1994**, *11*, 1159.
- [78] T. Prasad, V. Colvin, D. Mittleman, *Phys. Rev. B* **2003**, *67*, 165103.
- [79] F. Aieta, P. Genevet, N. Yu, M. A. Kats, Z. Gaburro, F. Capasso, *Nano Lett.* **2012**, *12*, 1702.
- [80] S. Vo, D. Fattal, W. V. Sorin, P. Zhen, T. Tho, M. Fiorentino, R. G. Beausoleil, *IEEE Photonics Technol. Lett.* **2014**, *26*, 1375.
- [81] J. Luo, B. Zeng, C. Wang, P. Gao, K. Liu, M. Pu, J. Jin, Z. Zhao, X. Li, H. Yu, X. Luo, *Nanoscale* **2015**, *7*, 18805.
- [82] M. I. Shalaev, J. Sun, A. Tsukernik, A. Pandey, K. Nikolskiy, N. M. Litchinitser, *Nano Lett.* **2015**, *15*, 6261.
- [83] F. Ding, Z. Wang, S. He, V. M. Shalaev, A. V. Kildishev, *ACS Nano* **2015**, *9*, 4111.
- [84] A. Shaltout, J. Liu, V. M. Shalaev, A. V. Kildishev, *Nano Lett.* **2014**, *14*, 4426.
- [85] D. Wang, Y. Gu, Y. Gong, C.-W. Qiu, M. Hong, *Opt. Express* **2015**, *23*, 11114.
- [86] R.-H. Fan, Y. Zhou, X.-P. Ren, R.-W. Peng, S.-C. Jiang, D.-H. Xu, X. Xiong, X.-R. Huang, M. Wang, *Adv. Mater.* **2015**, *27*, 1201.
- [87] J. Hao, Y. Yuan, L. Ran, T. Jiang, J. A. Kong, C. T. Chan, L. Zhou, *Phys. Rev. Lett.* **2007**, *99*, 063908.
- [88] C.-p. Huang, Q.-j. Wang, X.-g. Yin, Y. Zhang, J.-q. Li, Y.-y. Zhu, *Adv. Opt. Mater.* **2014**, *2*, 723.
- [89] A. Pors, M. G. Nielsen, S. I. Bozhevolnyi, *Opt. Lett.* **2013**, *38*, 513.
- [90] S.-C. Jiang, X. Xiong, Y.-S. Hu, Y.-H. Hu, G.-B. Ma, R.-W. Peng, C. Sun, M. Wang, *Phys. Rev. X* **2014**, *4*, 021026.
- [91] T. Li, H. Liu, S.-M. Wang, X.-G. Yin, F.-M. Wang, S.-N. Zhu, X. Zhang, *Appl. Phys. Lett.* **2008**, *93*, 021110.
- [92] T. Li, S. M. Wang, J. X. Cao, H. Liu, S. N. Zhu, *Appl. Phys. Lett.* **2010**, *97*, 261113.
- [93] J. Hao, J. Wang, X. Liu, W. J. Padilla, L. Zhou, M. Qiu, *Appl. Phys. Lett.* **2010**, *96*, 251104.
- [94] N. Liu, M. Mesch, T. Weiss, M. Hentschel, H. Giessen, *Nano Lett.* **2010**, *10*, 2342.
- [95] A. Pors, S. I. Bozhevolnyi, *Opt. Express* **2013**, *21*, 2942.
- [96] Z. H. Jiang, L. Lin, D. Ma, S. Yun, D. H. Werner, Z. Liu, T. S. Mayer, *Sci. Rep.* **2014**, *4*, 7511.
- [97] A. S. Schwanecke, A. Krasavin, D. M. Bagnall, A. Potts, A. V. Zayats, N. I. Zheludev, *Phys. Rev. Lett.* **2003**, *91*, 247404.
- [98] J. Elliott, I. I. Smolyaninov, N. I. Zheludev, A. V. Zayats, *Phys. Rev. B* **2004**, *70*, 233403.
- [99] Y. Ye, S. He, *Appl. Phys. Lett.* **2010**, *96*, 203501.
- [100] S. Wu, Z. Zhang, Y. Zhang, K. Zhang, L. Zhou, X. Zhang, Y. Zhu, *Phys. Rev. Lett.* **2013**, *110*, 207401.
- [101] N. K. Grady, J. E. Heyes, D. R. Chowdhury, Y. Zeng, M. T. Reiten, A. K. Azad, A. J. Taylor, D. A. R. Dalvit, H.-T. Chen, *Science* **2013**, *340*, 1304.
- [102] W. H. McMaster, *Am. J. Phys.* **1954**, *22*, 351.
- [103] W. H. McMaster, *Rev. Mod. Phys.* **1961**, *33*, 8.
- [104] D. Wen, F. Yue, S. Kumar, Y. Ma, M. Chen, X. Ren, P. E. Kremer, B. D. Gerardot, M. R. Taghizadeh, G. S. Buller, X. Chen, *Opt. Express* **2015**, *23*, 10272.
- [105] A. Pors, M. G. Nielsen, S. I. Bozhevolnyi, *Optica* **2015**, *2*, 716.
- [106] J. P. Balthasar Mueller, K. Leosson, F. Capasso, *Optica* **2016**, *3*, 42.
- [107] P. Genevet, J. Lin, M. A. Kats, F. Capasso, *Nat. Commun.* **2012**, *3*, 1278.
- [108] S. Mei, K. Huang, M. Q. Mehmood, H. Liu, F. Qin, Z. Xu, M. Hong, D. H. Zhang, J. Teng, A. Danner, C.-W. Qiu, *Nanoscale* **2015**, DOI: 10.1039/C5NR07374J.
- [109] E. D. Gabor, *Nature* **1948**, 161.
- [110] R. W. Gerchberg, O. Saxton, *Optik* **1972**, *35*, 237.
- [111] K. Huang, H. Gao, G. Cao, P. Shi, X. Zhang, Y. Li, *Appl. Opt.* **2012**, *51*, 5149.
- [112] G. Lazarev, A. Hermerschmidt, S. Krüger, S. Osten, in *Optical Imaging and Metrology*, (Eds: W. Osten, N. Reingand), Wiley-VCH, Weinheim, Germany **2012**, p. 1.
- [113] H. Butt, Y. Montelongo, T. Butler, R. Rajesekharan, Q. Dai, S. G. Shiva-Reddy, T. D. Wilkinson, G. A. J. Amaratunga, *Adv. Mater.* **2012**, *24*, OP331.
- [114] K. Huang, H. Liu, F. J. Garcia-Vidal, M. Hong, B. Luk'yanchuk, J. Teng, C.-W. Qiu, *Nat. Commun.* **2015**, *6*, 7059.
- [115] Y. Montelongo, J. O. Tenorio-Pearl, C. Williams, S. Zhang, W. I. Milne, T. D. Wilkinson, *Proc. Natl. Acad. Sci. USA* **2014**, *111*, 12679.
- [116] Y.-W. Huang, W. T. Chen, W.-Y. Tsai, P. C. Wu, C.-M. Wang, G. Sun, D. P. Tsai, *Nano Lett.* **2015**, *15*, 3122.

- [117] Y. Montelongo, J. O. Tenorio-Pearl, W. I. Milne, T. D. Wilkinson, *Nano Lett.* **2013**, *14*, 294.
- [118] M. Gu, *Advanced Optical Imaging Theory*, SpringerBerlin Heidelberg, Germany **2000**.
- [119] X. Li, T.-H. Lan, C.-H. Tien, M. Gu, *Nat. Commun.* **2012**, *3*, 998.
- [120] X. Li, H. Ren, X. Chen, J. Liu, Q. Li, C. Li, G. Xue, J. Jia, L. Cao, A. Sahu, B. Hu, Y. Wang, G. Jin, M. Gu, *Nat. Commun.* **2015**, *6*, 6984.
- [121] F. Zhou, Y. Liu, W. Cai, *Opt. Express* **2013**, *21*, 4348.
- [122] Y. Yifat, M. Eitan, Z. Iluz, Y. Hanein, A. Boag, J. Scheuer, *Nano Lett.* **2014**, *14*, 2485.
- [123] L. Huang, H. Mühlenbernd, X. Li, X. Song, B. Bai, Y. Wang, T. Zentgraf, *Adv. Mater.* **2015**, *27*, 6444.
- [124] B. Walthier, C. Helgert, C. Rockstuhl, F. Setzpfandt, F. Eilenberger, E.-B. Kley, F. Lederer, A. Tünnermann, T. Pertsch, *Adv. Mater.* **2012**, *24*, 6300.
- [125] G. Patrice, C. Federico, *Rep. Prog. Phys.* **2015**, *78*, 024401.
- [126] D. G. Grier, *Nature* **2003**, *424*, 810.
- [127] J. Wang, J.-Y. Yang, I. M. Fazal, N. Ahmed, Y. Yan, H. Huang, Y. Ren, Y. Yue, S. Dolinar, M. Tur, A. E. Willner, *Nat. Photonics* **2012**, *6*, 488.
- [128] N. Bozinovic, Y. Yue, Y. Ren, M. Tur, P. Kristensen, H. Huang, A. E. Willner, S. Ramachandran, *Science* **2013**, *340*, 1545.
- [129] J. P. Torres, L. Torner, *Twisted Photons: Applications of Light with Orbital Angular Momentum*, Wiley-VCH, Weinheim, Germany, **2011**.
- [130] S. W. Hell, *Science* **2007**, *316*, 1153.
- [131] L. B. Allen, S. M. Barnett, M. J. Padgett, *Optical Angular Momentum*, Institute of Physics, Bristol, UK **2003**.
- [132] J. H. Poynting, *Proc. R. Soc. London Ser. A* **1909**, *82*, 560.
- [133] C. G. Darwin, *Proc. R. Soc. London Ser. A* **1932**, *136*, 36.
- [134] R. A. Beth, *Phys. Rev.* **1936**, *50*, 115.
- [135] L. Allen, M. W. Beijersbergen, R. J. C. Spreeuw, J. P. Woerdman, *Phys. Rev. A* **1992**, *45*, 8185.
- [136] L. Allen, M. J. Padgett, M. Babiker, in *Progress in Optics*, Vol. 39 (Ed: E. Wolf), Elsevier, Amsterdam, The Netherlands **1999**, 291.
- [137] V. Y. Bazhenov, M. S. Soskin, M. V. Vasnetsov, *J. Mod. Opt.* **1992**, *39*, 985.
- [138] M. A. A. Neil, F. Massoumian, R. Juškaitis, T. Wilson, *Opt. Lett.* **2002**, *27*, 1929.
- [139] L. Marrucci, C. Manzo, D. Paparo, *Phys. Rev. Lett.* **2006**, *96*, 163905.
- [140] M. W. Beijersbergen, L. Allen, H. E. L. O. van der Veen, J. P. Woerdman, *Opt. Commun.* **1993**, *96*, 123.
- [141] J. Lin, P. Genevet, M. A. Kats, N. Antoniou, F. Capasso, *Nano Lett.* **2013**, *13*, 4269.
- [142] J. Leach, M. J. Padgett, S. M. Barnett, S. Franke-Arnold, J. Courtial, *Phys. Rev. Lett.* **2002**, *88*, 257901.
- [143] M. P. J. Lavery, D. J. Robertson, G. C. G. Berkhout, G. D. Love, M. J. Padgett, *J. Courtial, Opt. Express* **2012**, *20*, 2110.
- [144] X. Yin, Z. Ye, J. Rho, Y. Wang, X. Zhang, *Science* **2013**, *339*, 1405.
- [145] L. Huang, X. Chen, B. Bai, Q. Tan, G. Jin, T. Zentgraf, S. Zhang, *Light Sci. Appl.* **2013**, *2*, e70.
- [146] M. Khorasaninejad, K. B. Crozier, *Nat. Commun.* **2014**, *5*, 5386.
- [147] W. Luo, S. Xiao, Q. He, S. Sun, L. Zhou, *Adv. Opt. Mater.* **2015**, *3*, 1102.
- [148] J. Lin, J. P. B. Mueller, Q. Wang, G. H. Yuan, N. Antoniou, X. C. Yuan, F. Capasso, *Science* **2013**, *340*, 331.
- [149] S. Xiao, F. Zhong, H. Liu, S. Zhu, J. Li, *Nat. Commun.* **2015**, *6*, 8360.
- [150] J. Zhang, Z. Lei Mei, W. Ru Zhang, F. Yang, T. Jun Cui, *Appl. Phys. Lett.* **2013**, *103*, 151115.
- [151] N. M. Estakhri, A. Alù, *IEEE Antenn. Wirel. Propag. Lett.* **2014**, *13*, 1775.
- [152] L. Y. Hsu, T. Lepetit, B. Kante, *Prog. Electromagnetic Res.* **2015**, *152*, 33.
- [153] B. Orazbayev, N. Mohammadi Estakhri, M. Beruete, A. Alù, *Phys. Rev. B* **2015**, *91*, 195444.
- [154] X. Ni, Z. J. Wong, M. Mrejen, Y. Wang, X. Zhang, *Science* **2015**, *349*, 1310.
- [155] J. Arlt, V. Garces-Chavez, W. Sibbett, K. Dholakia, *Opt. Commun.* **2001**, *197*, 239.
- [156] A. Dogariu, S. Sukhov, J. Saenz, *Nat. Photonics* **2013**, *7*, 24.
- [157] V. Kajorndejnukul, W. Ding, S. Sukhov, C.-W. Qiu, A. Dogariu, *Nat. Photonics* **2013**, *7*, 787.
- [158] C. Pfeiffer, A. Grbic, *Phys. Rev. B* **2015**, *91*, 115408.
- [159] S.-H. Lee, Y. Roichman, D. G. Grier, *Opt. Express* **2010**, *18*, 6988.
- [160] O. Brzobohaty, V. Karasek, M. Siler, L. Chvatal, T. Cizmar, P. Zemanek, *Nat. Photonics* **2013**, *7*, 123.
- [161] V. Shvedov, A. R. Davoyan, C. Hnatovsky, N. Engheta, W. Krolikowski, *Nat. Photonics* **2014**, *8*, 846.
- [162] T. Li, S. Kheifets, M. G. Raizen, *Nat. Phys.* **2011**, *7*, 527.
- [163] P. Genevet, D. Wintz, A. Ambrosio, A. She, R. Blanchard, F. Capasso, *Nat. Nanotechnol.* **2015**, *10*, 804.
- [164] A. Silva, F. Monticone, G. Castaldi, V. Galdi, A. Alù, N. Engheta, *Science* **2014**, *343*, 160.
- [165] A. Pors, M. G. Nielsen, S. I. Bozhevolnyi, *Nano Lett.* **2015**, *15*, 791.
- [166] G. Li, S. Chen, N. Pholchai, B. Reineke, P. W. H. Wong, E. Y. B. Pun, K. W. Cheah, T. Zentgraf, S. Zhang, *Nat. Mater.* **2015**, *14*, 607.
- [167] P. K. Jha, X. Ni, C. Wu, Y. Wang, X. Zhang, *Phys. Rev. Lett.* **2015**, *115*, 025501.
- [168] Y. Hadad, D. L. Sounas, A. Alu, *Phys. Rev. B* **2015**, *92*, 100304.
- [169] G. Ma, M. Yang, S. Xiao, Z. Yang, P. Sheng, *Nat. Mater.* **2014**, *13*, 873.
- [170] Y. Xie, W. Wang, H. Chen, A. Konneker, B.-I. Popa, S. A. Cummer, *Nat. Commun.* **2014**, *5*, 5553.
- [171] D. Costantini, A. Lefebvre, A. L. Coutrot, I. Moldovan-Doyen, J. P. Hugonin, S. Boutami, F. Marquier, H. Benisty, J. J. Greffet, *Phys. Rev. Appl.* **2015**, *4*, 014023.
- [172] X. Liu, Z. Zhang, *ACS Photonics* **2015**, *2*, 1320.
- [173] M. Wuttig, D. Lusebrink, D. Wamwangi, W. Welnic, M. Gilleszen, R. Dronskowski, *Nat. Mater.* **2007**, *6*, 122.
- [174] A.-K. U. Michel, D. N. Chigrin, T. W. W. Maß, K. Schönauer, M. Salinga, M. Wuttig, T. Taubner, *Nano Lett.* **2013**, *13*, 3470.
- [175] Y. Chen, X. Li, Y. Sonnefraud, A. I. Fernández-Domínguez, X. Luo, M. Hong, S. A. Maier, *Sci. Rep.* **2015**, *5*, 8660.
- [176] A. Tittl, A.-K. U. Michel, M. Schäferling, X. Yin, B. Gholipour, L. Cui, M. Wuttig, T. Taubner, F. Neubrech, H. Giessen, *Adv. Mater.* **2015**, *27*, 4597.
- [177] D. Wang, L. Zhang, Y. Gu, M. Q. Mehmood, Y. Gong, A. Srivastava, L. Jian, T. Venkatesan, C.-W. Qiu, M. Hong, *Sci. Rep.* **2015**, *5*, 15020.
- [178] D. Y. Lei, K. Appavoo, F. Ligmajer, Y. Sonnefraud, R. F. Haglund, S. A. Maier, *ACS Photonics* **2015**, *2*, 1306.
- [179] Y. Yao, R. Shankar, M. A. Kats, Y. Song, J. Kong, M. Loncar, F. Capasso, *Nano Lett.* **2014**, *14*, 6526.
- [180] Z. Fang, Y. Wang, A. E. Schlather, Z. Liu, P. M. Ajayan, F. J. García de Abajo, P. Nordlander, X. Zhu, N. J. Halas, *Nano Lett.* **2014**, *14*, 299.
- [181] J. Sautter, I. Staude, M. Decker, E. Rusak, D. N. Neshev, I. Brener, Y. S. Kivshar, *ACS Nano* **2015**, *9*, 4308.
- [182] Y. H. Fu, A. Q. Liu, W. M. Zhu, X. M. Zhang, D. P. Tsai, J. B. Zhang, T. Mei, J. F. Tao, H. C. Guo, X. H. Zhang, J. H. Teng, N. I. Zheludev, G. Q. Lo, D. L. Kwong, *Adv. Funct. Mater.* **2011**, *21*, 3589.
- [183] M. Fusheng, Y.-S. Lin, X. Zhang, C. Lee, *Light Sci. Appl.* **2014**, *3*, e171.
- [184] X. Ma, W. Pan, C. Huang, M. Pu, Y. Wang, B. Zhao, J. Cui, C. Wang, X. Luo, *Adv. Opt. Mater.* **2014**, *2*, 945.
- [185] P. A. Franken, A. E. Hill, C. W. Peters, G. Weinreich, *Phys. Rev. Lett.* **1961**, *7*, 118.
- [186] M. A. Kats, R. Blanchard, P. Genevet, F. Capasso, *Nat. Mater.* **2013**, *12*, 20.
- [187] J. S. Clausen, E. Højlund-Nielsen, A. B. Christiansen, S. Yazdi, M. Grajower, H. Taha, U. Levy, A. Kristensen, N. A. Mortensen, *Nano Lett.* **2014**, *14*, 4499.